Characterization of a novel RP2-OSTF1 interaction and its implication for actin remodeling

Characterization of a novel RP2-OSTF1 interaction and its implication for actin remodeling

Rodanthi Lyraki[1*], Mandy Lokaj[2*], Dinesh C. Soares[1], Abigail Little[1], Matthieu Vermeren[1,3], Joseph A. Marsh[1], Alfred Wittinghofer[2], Toby Hurd[1#].

1) MRC Human Genetics Unit, Institute of Genetics and Molecular Medicine, University of Edinburgh, Western General Hospital, Crewe Road, EH4 2XU, UK.
2) Structural Biology Group, Max-Planck Institut für Molekulare Physiologie, Abteilung Strukturelle Biologie, Otto-Hahn-Str. 11, 44227, Dortmund, Germany.
3) MRC Centre for Inflammation Research, The Queen's Medical Research Institute, University of Edinburgh, 47 Little France Crescent, EH16 4TJ, UK.

*These authors contributed equally to this manuscript

[#] Corresponding author - toby.hurd@igmm.ed.ac.uk

JCS Advance Online Article. Posted on 12 January 2018

Abstract

Retinitis pigmentosa 2 (*RP2*) is the causative gene for a form of X-linked retinal degeneration. RP2 was previously shown to have GAP activity towards the small GTPase ARL3 via its N-terminus, but the function of the C-terminus remains elusive. Here, we report a novel interaction between RP2 and Osteoclast-stimulating factor 1 (OSTF1), an intracellular protein that indirectly enhances osteoclast formation and activity and is a negative regulator of cell motility. Moreover, this interaction is abolished by a human pathogenic mutation in RP2. We utilized a structure-based approach to pinpoint the binding interface to a strictly conserved cluster of residues on the surface of RP2 that spans both the C- and N- terminal domains of the protein, and which is structurally distinct from the ARL3 binding site. In addition, we show that RP2 is a positive regulator of cell motility *in vitro*, recruiting OSTF1 to the cell membrane and preventing its interaction with the migration regulator Myo1E.

Introduction

Retinitis pigmentosa 2 (*RP2*) is mutated in 7-18% of patients suffering from X-linked Retinitis pigmentosa (XLRP), a severe and untreatable form of progressive retinal degeneration. RP collectively represents a heterogeneous group of retinal degenerative disorders marked by photoreceptor loss and is a leading cause of inherited blindness affecting 1:3000-1:7000 people worldwide[1,2]. RP2 is a 350-residue protein whose expression at the protein level is not restricted to the retina but is also expressed in a wide range of tissues including the brain and the kidney (Proteomics database, https://www.proteomicsdb.org). Structurally, RP2 encompasses two distinct domains which appear to serve distinct roles[3]. The N-terminal β-helix domain is homologous to Tubulin Cofactor C (TBCC), and the C-terminal ferredoxin α/β domain displays similarity to Nucleoside Diphosphate Kinases (NDPK)[3]. RP2 is predominantly targeted to the plasma membrane due to dual acylation of its N-terminus[4,5]; this subcellular localization of RP2 is important for its function and is pathologically relevant[6]. Notably, RP2 is also associated to primary cilia and the specialized connecting cilia of the photoreceptors, both in terms of localization and function[7-9].

While several proteins have been reported to interact with RP2, the most well-characterized interaction partner is ARL3, a small GTPase with suggested roles in the intracellular trafficking of ciliary proteins[10-13], loss of which leads to photoreceptor degeneration and renal ciliopathy in mice[14,15]. We previously revealed the crystal structure of RP2 coupled to ARL3, demonstrating that the interaction of the two proteins is mediated exclusively by the N-terminal domain of RP2 and that RP2 displays GTPase-activating protein (GAP) activity against ARL3, stimulating its GTP hydrolysis by several orders of magnitude[16].

The disruption of the RP2-ARL3 complex is clearly a major contributor to the development of retinal degeneration, not only because the ARL3 binding interface on RP2 is a mutational hotspot[17], but also because an ARL3 mutation was recently described to cause autosomal dominant RP[18]. The most well-characterized function of the complex is in intracellular trafficking pathways for lipid-modified retinal and general ciliary proteins. In particular, structural and biochemical studies have proven the ability of GTP-bound ARL3 to allosterically displace protein cargo from chaperones PDE6δ and UNC119, which bind and solubilize lipid-modified membrane-anchored proteins such as NPHP3 and Rheb[12,13]. Animal model studies have linked this function of ARL3 with the correct targeting of lipid-modified phototransduction proteins, such as the prenylated PDE6 holoenzyme, rhodopsin kinase GRK1 and acylated transducin Tα, to the photoreceptor connecting cilium[15]. It is therefore believed that RP2 has a role in the regulation of intracellular shuttling of those proteins, via its ability to stimulate ARL3 GTP hydrolysis[19]. ARL13B, mutated in Joubert's syndrome, was recently identified as a GEF for ARL3, completing the cycle of GTPase regulation by stimulating GDP to GTP exchange[9]. It is believed that a gradient of ARL3 GTP- and GDP- bound forms is created in ciliated cells due to the combination of ARL13B's exclusive localization inside the ciliary axoneme and RP2's presence at the basal body, which ensures release of lipid-modified cargo within the correct locations[9].

However, other studies report different phenotypes associated with RP2 loss that might be independent of its function in this pathway, such as global post-Golgi transport of proteins and targeting of opsins to the connecting cilium[8,20]. In addition,

ARL3 was recently described as an interaction partner of STAT3, suggesting a new role for RP2 in the regulation of transcription[21].

Fundamental questions remain unanswered in the field. For example, given the wide tissue distribution of RP2, it is reasonable to ask whether RP2's function is restricted to the photoreceptor connecting cilia and primary cilia or if it has other functions elsewhere. Furthermore, while the function of the N-terminal, TBCC-like domain of RP2 has been well characterised as the binding interface for the interaction with ARL3 and the catalytic centre of the protein, the C-terminus has been poorly characterised with no currently known function. It is known that although it shares weak sequence homology with NDPK, the C-terminal domain of RP2 does not possess kinase activity as key catalytic residues are not conserved[3]. Apart from a report attributing DNA binding and exonuclease activity to this domain[22], and another report that it contributes to the overall protein stability[17], it has been generally assumed, without any experimental evidence, that the domain participates in protein-protein interactions[3]. In this study, we report a novel interaction between RP2 and OSTF1, a 214-residue protein that was initially identified in a screen for molecules whose overexpression leads to the secretion of factors that indirectly stimulate osteoclast maturation and bone resorption in culture[23]. Expression of OSTF1 at mRNA and protein level has been detected in several human tissues including the retina[23] (Proteomics database, https://www.proteomicsdb.org). The exact function of this molecule is yet unknown, but it has been suggested to be an adaptor for c-Src's function in the actin cytoskeleton[24]. It was also recently identified as a negative regulator of cell motility in cancer cell lines, under control of the ERK1/2 pathway[25]. OSTF1 exerts this effect by acting as a cytoplasmic anchor for long-tailed type 1 Myosin, Myo1E, preventing it from localizing to sites of actin nucleation in lamellipodia[25,26]. We conducted structural and biochemical analyses to characterize the RP2-OSTF1 interaction and show that the interaction interface on RP2 does not overlap with the ARL3 binding interface and that the formation of a trimeric RP2-OSTF1-ARL3 complex is possible. In addition, we show that the OSTF1 binding interface spans both the C- and N- terminal domains of the protein and that the residues that participate in the interaction belong to a surface "patch" on RP2 that displays remarkable conservation status among vertebrates, arguing for major functional significance. Finally, we provide evidence that RP2 functions as a

regulator of OSTF1's ability to influence cell motility, via modulating the availability of OSTF1 to interact with Myo1E.

Results

OSTF1 is a novel interaction partner of RP2

To look for novel RP2 functions through the identification of novel interaction partners, we conducted a yeast two-hybrid screen by using human full-length RP2 as the bait protein. Of 91 clones, 41 encoded full-length OSTF1 (Figure 1a). Direct interaction between OSTF1 and RP2 was confirmed in two directions in a targeted yeast two-hybrid assay (Figure 1b). OSTF1 is a 214-residue protein consisting of an N-terminal proline-rich region, a Src-homology 3 domain (SH3), 4 ankyrin repeats (ANK) and a well-conserved acidic amino acid cluster at the C-terminus. Coimmunoprecipitation (co-IP) confirmed the interaction between exogenously expressed OSTF1 and RP2 in HEK293T cells (Figure 1c). In addition, the interaction was confirmed by reciprocal pulldown analyses in bovine retinal extracts using recombinant GST-RP2 or GST-OSTF1 as bait proteins (Figure 1d). To determine the thermodynamic parameters of the RP2-OSTF1 interaction in solution, we conducted isothermal titration calorimetry (ITC) using full-length RP2 and full-length His-tagged OSTF1 (Figure 1e). ITC analysis showed robust complex formation with 1:1 stoichiometry; the equilibrium association constant of the interaction was derived as 5.28 µM and the reaction is exothermic with an enthalpic contribution of ~7.473 kcal/mol. Moreover, indirect fluorescence polarisation experiments in which an equimolar complex of fluorescently labelled small GTPase ARL3-mantGppNHp (a non-hydrolysable GTP analog) with RP2 was titrated with increasing amounts of full-length (OSTF1FL) showed an affinity of OSTF1FL to RP2 of 0.672 µM (Supplementary table 1).

OSTF1 binding does not affect the interaction of RP2 with ARL3 or its GAP activity

In order to investigate if OSTF1 acts as a regulator of RP2 activity, we used fluorescence polarization (FP) analysis to assess if OSTF1 modulates the binding affinity of RP2 to ARL3 or its catalytic activity *in vitro*. For this purpose, we used full-length RP2 and OSTF1-His as well as the G domain of ARL3 (residues 18-177)

fluorescently labelled with mantGppNHp (a non-hydrolysable GTP analog). RP2 was previously shown by us[16] to bind to ARL3-mantGppNHp and ARL3-mantGDP/AlFx with higher affinity than to ARL3-mantGDP (Supplementary table 1). An increase in FP signal of ARL3-mantGppNHp is observed upon addition of RP2 followed by a further increase upon addition of OSTF1 (Figure 2a). As OSTF1 does not bind directly to either ARL3-mantGDP or ARL3-mantGppNHp (Figure 2b), we assume that OSTF1 and ARL3 can bind simultaneously on RP2 to form a trimeric complex.

The affinity of RP2 to ARL3-mantGppNHp did not change depending on the absence and presence of saturating concentrations of OSTF1 (Supplementary table 1). Therefore, OSTF1 does not inhibit or compromise the RP2-ARL3 complex formation and might also be functionally independent. Moreover, a stable quadruple complex seems to be able to be formed with the ARL3 effector, UNC119a (Supplementary figure 1).

We next investigated if the presence of OSTF1 affects the stimulation of ARL3 GTP hydrolysis by catalytic concentrations of RP2 in a charcoal assay. ARL3 was loaded with radioactively labelled ^{32}P GTP. The GAP activity was monitored by hydrolysis and release of ^{32}P leading to an increase in the radioactive signal, as described before[16]. We found that OSTF1 does not influence the intrinsic GTP hydrolysis rate of ARL3 or the GAP activity of RP2 (Figure 2c).

The N-terminal domain of RP2 and both the SH3 and ANK domains of OSTF1 participate in the interaction

Since OSTF1 does not compete with ARL3 for binding to RP2, we next asked whether it binds exclusively to the C-terminal NDPK-like domain of RP2. To conduct this domain analysis of the RP2-OSTF1 interaction, we used RP2 and OSTF1 deletion constructs (Figure 3a) in analytical gel filtration experiments. First, we confirmed that full-length RP2 and OSTF1-His complex formation can be detected with this method, since the complex, being larger, elutes from the stationary phase earlier than the monomeric proteins (Figure 3b, left). Next, we repeated the assay using an N-terminal deletion construct of RP2 (RP2 ΔN, residues 230-350) and showed that the C-terminal domain alone cannot form a complex with OSTF1 (Figure 3b, right). However, deletion of only 34 residues from the N-terminus (a flexible region of RP2 that is essential for

the interaction with ARL3[16]) does not affect complex formation (Supplementary figure 2). Subsequently, we tested the binding of RP2 to OSTF1 deletion constructs (Figure 3c). Interestingly, deletion of amino acids 1-74 comprising the SH3 domain of OSTF1 (OSTF1 ΔN), as well as deletion of amino acids 74-214, the ANK repeats domain (OSTF1 ΔC), both abolish complex formation, showing that both SH3 and ANK domains of OSTF1 take part in the interaction (Figure 3c). This was further confirmed by pulldown assays from HEK293T cell lysates using GST-tagged OSTF1 constructs as bait (Figure 3d). While the ΔC OSTF1 construct cannot form a complex with RP2, it can still pulldown endogenous c-Cbl, in accordance with previous studies[24].

The RP2-OSTF1 interaction interface spans both domains of RP2 and is strictly conserved among vertebrates

Although most *RP2* mutations found in patients likely lead to null alleles due to severely compromised or absent RP2 expression, caused by either mRNA degradation or destabilized protein structure, missense mutations have been reported which do not affect the expression and overall stability of RP2, according to biochemical studies, *in silico* predictions or circular dichroism spectroscopy[3,16,17]. Among them, R118H and E138G are known to severely impact the RP2-ARL3 interaction and thus affect the GAP activity of RP2[16]. G2A and C3S mutations lead to altered RP2 localization by impairing dual acylation at its extreme N-terminus[4]. It is apparent that pathogenic missense RP2 mutations that are predicted to be non-destabilizing often occur on important residues that mediate critical interactions or modifications and, therefore, can be particularly informative about the function of the protein. An exception might be R282W which has been suggested to be a low-frequency polymorphism even though it has been identified in RP patients[27,28].

In order to assess the importance of the RP2-OSTF1 interaction for the function of RP2, we tested the effect of six of these mutations (G2A, C3S, R118H, E138G, R211L, R282W) on the interaction. We conducted GST pulldown analyses using recombinant full-length GST-OSTF1 as bait in lysates of HEK293T cells expressing either wild-type or mutant RP2 with a V5 tag and identified R211L as a mutation that completely abolishes the RP2-OSTF1 interaction (Figure 4a). Interestingly, R211 is not known to participate in ARL3 binding as it resides within a spatially distinct

region. Upon multiple sequence alignment of human RP2 with a range of divergent orthologues (from 38% identity with the choanoflagellate *Salpingoeca* to 94% identity with Mole rat), it is apparent that the R211 position is strictly conserved among vertebrates, but not entirely conserved among non-vertebrate chordates and non-chordates (Figure 4b). Hence, for the subsequent conservation analyses, only the vertebrate subphylum was used.

Because R211 lies away from the ARL3 interaction interface on the opposite face of the GAP-domain, we hypothesized that this area of the protein along the C-terminal NDPK-like domain might form the binding interface for the RP2-OSTF1 interaction. To test this, we mapped the binding interface on the surface of RP2 using a targeted RP2 structure-guided mutagenesis approach and testing the effect of missense mutations on the OSTF1 binding. Residues to be mutated were based on a comprehensive *in silico* analysis of the conservation status among vertebrates, the surface properties, the proximity of the residues to R211 as well as the potential of post-translational modifications (Figure 4c, d). Electrostatic properties and hydrophobicity of residues were taken into account when choosing which residues to mutate, as highly charged and/or exposed hydrophobic amino acids often participate in protein-protein interactions (Supplementary figure 3). In addition, structurally and functionally important regions in proteins typically appear as patches of evolutionarily conserved residues that are spatially close to each other[29]. To assess the effect of missense RP2 mutations on the RP2-OSTF1 interaction, we expressed V5-tagged wild-type and mutant forms of RP2 in HEK293T cells and used the lysates for pulldown assays using GST-OSTF1 as bait. All the mutations generated were not predicted to affect the overall stability of the protein (Supplementary table 2) and were, indeed, expressed at wild-type levels. As an additional control to ensure that the absence of RP2 in the pulldown samples is specifically due to the loss of the RP2-OSTF1 interaction and not an unspecific effect of destabilized secondary structure or folding, we conducted pulldown assays using GST-ARL3 Q71L as bait and confirmed that none of the mutations impaired the RP2-ARL3 interaction, as was predicted. Using this approach, we identified three more residues whose substitution severely impacts on the RP2-OSTF1 interaction: Y245, D255 and K160 (Figure 4c). While the K160A substitution which abolishes the positive charge has a mild impact on the RP2-OSTF1 interaction, the K160E substitution which reverses the charge

severely impairs the interaction. This confirms an important role for K160 on the interaction interface. Moreover, we have noted that substituting K252 also affects the RP2-OSTF1 interaction, albeit to a lesser extent.

Sequence conservation and variation was mapped on the surface of RP2 showing two highly conserved clusters of residues on the RP2 surface, one that forms the ARL3 binding site within the N-terminal β-helix domain and a second cluster located on the opposite face of the molecule that spans both the β-helix domain and the C-terminal NDPK-like domain (Figure 4d). Residues Y245, D255 and K160 were localized to this second conserved cluster. Therefore, it is likely that this area forms the interaction interface with OSTF1. Since all identified residues are strictly conserved among vertebrates (Figure 4d), we suggest that the interaction occurs widely among vertebrates and thus has an important function that merits further examination.

Based on the characterisation of the RP2-OSTF1 interaction presented here, and the known structures of both proteins, we used a macromolecular docking strategy in order to build a 3D model of the RP2-OSTF1 complex. Although our experiments do not tell us the specific interacting OSTF1 residues, they do reveal that both the N- and C-terminal domains participate in the interaction. Thus, we performed a series of docking calculations whereby the interaction was centred around different residues on the surface of OSTF1, and then evaluated models for their compatibility with the mutagenesis data (see Methods). Although there were multiple models compatible with the experimental data, we observed a single dominant cluster of structural similar models (Figure 5). Moreover, the binding surface on OSTF1 for this dominant cluster was highly conserved, whereas all other compatible docking models involved poorly conserved regions of the OSTF1 surface (Supplementary Figure 4), thus strongly suggesting that this model is reflective of the actual complex.

RP2 recruits OSTF1 to the plasma membrane and regulates cell motility

A function that has been previously attributed to OSTF1 in cancer cell lines is the regulation of cell motility. In particular, OSTF1 negatively regulates cell motility in an ERK1/2 pathway-dependent manner via the regulation of the intracellular localization of Myo1E, with whom it directly interacts[25,26]. In order to test if RP2 also has a role in cell motility, we used the CRISPR-Cas9 genome editing method to generate clonal

RP2 null cell lines using immortalized human retinal pigment epithelial cells (hTERT-RPE1). hTERT-RPE1 cells were chosen because they are motile in cell culture, have a stable diploid karyotype and are of retinal origin. Two clones (G,I) have distinct 2bp deletions in exon 2 which lead to complete absence of RP2 expression (Figure 6a). Comparison of the motility of parental RPE1 cells and *RP2* null clones demonstrated that cells that lack RP2 expression are less motile in both wound healing and random migration assays (Figure 6 b,c). Live cell imaging of individual cells in the random migration assay revealed a lack of directionality in their movement and the inability to form proper lamellipodia-like extensions (Figure 6c). Since OSTF1 was previously identified as regulating cell motility, we asked if RP2 regulates OSTF1 expression, especially since its target ARL3 was recently identified as an activator of STAT3 transcription factor[21]. However, this appears not to be the case as OSTF1 protein expression remained unchanged in all control and *RP2* knockout cells (Figure 6a).

To examine if RP2 exerts a positive impact on cell motility by modulating OSTF1 localization, biochemical fractionation was performed in HEK293T cells. This showed that overexpression of RP2 causes translocation of a pool of endogenous OSTF1 from the cytoplasm to the membrane fraction (Figure 7a). Similarly, by immunofluorescence, overexpression of RP2-EmGFP in HeLa cells leads to the recruitment of V5-OSTF1 to the cell membrane, where they co-localize (Figure 7b). On the contrary, overexpression of the RP2 G2A pathogenic mutant, which does not display the plasma membrane localization of the wild-type protein[4], does not recruit OSTF1 to the membrane compartment, as shown by subcellular fractionation and immunofluorescence (Supplementary figure 5a, b). We hypothesized that by recruiting OSTF1 to the membrane, RP2 prevents it from interacting with Myo1E, thus promoting cell motility. To test this hypothesis, we used HEK293T cells transiently overexpressing FLAG-OSTF1/empty vector or FLAG-OSTF1/RP2-V5 for anti-V5 immunoprecipitations and observed that less Myo1E associated with FLAG-OSTF1 when RP2 was overexpressed (Figure 7c and supplementary figure 6). The interaction of Myo1E and OSTF1 has been shown to be disrupted by ERK-mediated phosphorylation of OSTF1 S202. Serum stimulation and subsequent ERK activation did not impair the ability of endogenous OSTF1 to co-IP with RP2 (figure 7d). This

suggests that RP2 interaction with OSTF1 is distinct to the OSTF1-Myo1E interaction.

Discussion

Studies on the function of RP2 have so far mainly focused on its role in intracellular protein trafficking, coordinated via the GAP activity of its N-terminal domain towards the small GTPase ARL3. However, the existence of non-canonical roles of RP2 in the retina or other tissues has not been fully explored. In addition, the functionality of the C-terminal, NDPK-like domain of RP2 has not been elucidated. In order to discover novel RP2 functions, we sought to identify novel interaction partners by conducting a yeast two-hybrid screen. We identified OSTF1 as a novel direct interaction partner and confirmed the interaction by co-IP from HEK293T cells and pulldown assays from bovine retinal extracts. Subsequently to our discovery, the interaction was recently identified in a large-scale study of the human interactome, further validating the interaction[30]. OSTF1 has been associated with osteoclast differentiation[23,31] and the regulation of cell motility[25,26], but not with retinal processes. We investigated the potential relationship of this interaction with the ARL3 regulation pathway and found that OSTF1 and ARL3 can simultaneously bind on RP2 to create a trimeric complex. These results suggest that OSTF1 does not antagonize ARL3 for binding to RP2 and it is unlikely that this newly identified partner is a negative or positive regulator of the RP2 GAP activity, at least *in vitro*. Moreover, we screened several non-destabilizing missense RP2 mutations for their ability to interact with OSTF1 and found that the R211L mutation entirely abolishes the interaction potentially implicating OSTF1 in the pathogenesis of XLRP2. As R211 is found on a spatially distinct surface of RP2 than the ARL3 interaction interface and on a previously uncharacterized RP2 region, this prompted us to follow a site-directed mutagenesis approach, producing strictly non-destabilizing missense mutations, to map the interaction interface, which led to the identification of three more residues that are essential for the interaction to occur. The identified residues are good candidates for participating in a protein-protein interaction. For example, although the surface of RP2 is predominantly negatively charged and, like OSTF1, has an acidic theoretical pI, R211 residue belongs to a streak of positively charged residues on the surface of RP2, which suggests the occurrence of oppositely

charged interactions (Supplementary figure 3). On the other hand, Y245 has an exposed aromatic side-chain and belongs to a hydrophobic cluster at the inter-domain junction of RP2 (Supplementary figure 3). Also, this hydrophobic cluster lies within a noticeable surface cavity. Based on our results, we propose that OSTF1 binds to a cluster of residues on the RP2 surface that are strictly conserved among vertebrates and distinct from the ARL3 interaction interface. This conservation analysis hints on an important function of the interaction among vertebrates that is most likely distinct from the ARL3 regulation pathways.

OSTF1 is known to exert a negative effect on cell motility through its direct interaction with Myo1E, which leads to Myo1E being "anchored" to the cytoplasm and prevents it from translocating to sites of actin nucleation in lamellipodia, an event which is essential for their proper formation[26]. The OSTF1-Myo1E interaction is regulated by phosphorylation of OSTF1 by RSK1 under direct control of the ERK1/2 pathway; activation of ERK and PI3K signaling pathways is long known to be required for actin polymerization and subsequent lamellipodium formation[32]. Here we report another way of regulating the negative effect which OSTF1 exerts on cell motility: RP2 overexpression results in OSTF1 recruitment to the plasma membrane, leading to less OSTF1 being available for interaction with Myo1E. It will be interesting to study which signaling pathway activates RP2 to act as an OSTF1 regulator, an effect that is simulated by RP2 overexpression in our experiments.

Myo1E is a long-tailed class I myosin which has been suggested to physically connect actin to the plasma membrane and thus generate plasma membrane tension[33]. Its deletion in mice leads to defects in kidney filtration[34] and it has also been associated with poor outcome in breast cancer patients and identified as a tumor promoter in a mouse study[35]. Moreover, Myo1E has a role in coordinating actin assembly and trafficking in clathrin-mediated endocytosis[36]. The potential role of RP2 in those processes needs to be clarified further. Interestingly, disruption of actin turnover is observed upon knockout of another XLRP gene, *RPGR*, suggesting that actin dysregulation may contribute to the pathology on *RP2* patients[37]. Besides, it is important to note that a dynamic organization of the acto-myosin cytoskeleton is a prerequisite for most RPE functions in the retina, and many classes of non-muscle myosins are implicated in them (e.g., Myosins VIIa, Va in phagocytosis, Myosin II in melanosome aggregation)[38].

An important question that arises from our study is whether the RP2-OSTF1 interaction participates in ciliary traffic and is relevant for RP pathogenesis, or whether it has a non-canonical function in a different context/tissue. One hypothesis is that there are two distinct RP2 functions, the regulation of ciliary traffic via the ARL3 interaction in post-mitotic cells, and the regulation of OSTF1 localization and cell motility in dividing cells where cilia are retracted. One the other hand, the two functions of RP2 might be related. Interestingly, ARL13B mutant mice show a defect in directional migration of interneurons of the cerebral cortex[39], while knockdown of ARL3 impairs the migrational capacity of HeLa cells[21]. Future studies should also examine whether OSTF1 in its turn affects RP2 localization be preventing its localization to the ciliary axoneme.

Given that R211L is not predicted to destabilize RP2's folding by *in silico* analyses[17], our data suggest that loss of the RP2-OSTF1 interaction may lead to retinal degeneration. This could be tested in the future by using CRISPR-mediated genome editing to introduce R211L and other mutations that disrupt the RP2-OSTF1 interaction (such as Y245F) into mice and examining the retinal phenotype. Examination of expression data from the Fantom 5 project (http://fantom.gsc.riken.jp) shows that OSTF1 is expressed in both embryonic and adult eyes in mice and more specifically in both the retina and retinal pigmented epithelia in humans. More research will be needed to determine the cellular expression pattern of OSTF1 in the retina.

The RP2 protein has come into the spotlight because of the devastating effect of its mutations in the viability of photoreceptors, leading to one of the most early-onset and severe forms of RP. However, a multitude of different and often conflicting studies point to a multifunctional protein with more than one role in cellular biology[40]. RP2 disease also presents with a distinct set of symptoms that often deviate from the classic clinical image that characterises RP patients[41]. Gene augmentation therapy is perhaps the strategy that is closest to the clinic for RP, having already proven its safety in LCA patients[42]. In fact, gene augmentation therapy has already successfully prevented degeneration in a mouse RP2 KO model[43]. However, a thorough understanding of protein's functions are essential and non-canonical functions of RP2 must be taken into account, in order to prevent adverse effects and aid the development of complementary therapies before a therapeutic approach can

reach the clinic. Our study presents a novel aspect of RP2 function and thus contributes to that direction.

Methods

Yeast two hybrid

For the yeast two hybrid screen, the ProQuest™ Two-Hybrid system (Thermo Fisher) according to the manufacturer's instructions. In brief, the full length human RP2 *orf* was cloned into the pDEST32 bait plasmid. This was transformed into *S. cerevisiae* MaV203 yeast cells. These cells were subsequently transformed with the ProQuest™ Human Kidney 3-frame cDNA library according to the manufacturer's instructions. For co-transformation assays, the RP2 and OSTF1 *orf*s were cloned into both the pDEST 32 bait and pDEST22 prey plasmids. Interaction of bait and prey molecules were tested by growth of yeast cells on selective medium containing 75 mM 3-amino 1,2,4,-triazole but lacking leucine, tryptophan, and histidine and by LacZ-assays with filter-immobilized cells.

Generation of *RP2* null RPE1 Cells

Nickase paired guide sequences were identified in exon 2 of human *RP2* using the Zhang lab CRISPR design tool (crisp.mit.edu). Two paired guide sequences (Guide A – tcaaatttggatgttttcaa and Guide B – tttgaggaagactcaatgat) were cloned into pX461 and pX462 CRISPR plasmids respectively. These plasmids were co-transfected into RPE1-hTERT cells and 24 hours later subjected to 24hr selection in 5ug/ml Puromycin containing media to select for cells transfected with pX462. After 24hrs selection individual GFP-positive cells were FACS-sorted into individual wells of a 96 well plate to select for cells transfected with pX461. After expansion, 20 clones were sanger sequenced (sequencing primers: ggacccgtgaaaggcagcgtg and cctgacacaggtgtaaagtcatgaatgttactcc) and clones harbouring deleterious mutations kept together with clones harbouring no mutations as controls.

Immunofluorescence

For IF experiments, cells were seeded onto acid etched coverslips and transiently transfected. Cells were fixed in 4%PFA/PBS for 10 minutes, washed and then permeabilised with 0.1%Triton-X100 for 5 minutes. Cells were blocked in 10% goat

serum (Sigma) in PBS for 1 hour. Primary antibodies were applied in blocking buffer for 1 hour at room temperature. Cells were washed in PBS prior to incubation with Alexa Fluor®-conjugated goat secondary antibodies (Thermo Fisher) for a further hour at room temperature. Finally cells were mounted onto slides using ProLong® Gold antifade mountant (Thermo Fisher). Slides were imaged on a Leica SP2 inverted confocal microscope.

Site-directional mutagenesis

Point mutations were introduced in the human RP2 coding sequence using QuikChange II Site-Directed Mutagenesis kit following the manufacturer's instructions. Briefly, pENTR/D-TOPO entry vector (Invitrogen) containing the wild-type human RP2 coding sequence was used as a template in PCR reaction using the following primers: AAGATACTTAGCCCTGCATCTGCGAACTGGAAAGCTAATTCAGG,CCTGAATTAG CTTTCCAGTTCGCAGATGCAGGGCTAAGTATCTT(K160A),TCCTATACCTACTAC CGCAGAGCTCAAAGCTGTTC,GAACAGCTTTGAGCTCTGCGGTAGTAGGTATAG GA(E205A),TATACCTACTACCGAAGCGCTCAAAGCTGTTCGTG,CACGAACAGCT TTGAGCGCTTCGGTAGTAGGTATA (E206A),GCTTAGTGGTATTATTTGCTGGTGATGCCACTATTGCAAATGCCAGAAA AC,GTTTTCTGGCATTTGCAATAGTGGCATCACCAGCAAATAATACCACTAAGC(Y 245A),CCTACTACCGAAGAGCTCGCAGCTGTTCGTGTTTCCAC,GTGGAAACACG AACAGCTGCGAGCTCTTCGGTAGTAGG(K208A),TTTCCACAGAAGCCAATAGCA GCATTGTTCCAATATCCC,GGGATATTGGAACAATGCTGCTATTGGCTTCTGTGG AAA(R218S),CTCAAAGCTGTTCGTGTTGCCACAGAAGCCAATAG,CTATTGGCTT CTGTGGCAACACGAACAGCTTTGAG(S213A),CTGTTCGTGTTTCCACAGCAGCC AATAGAAGCATTGT,ACAATGCTTCTATTGGCTGCTGTGGAAACACGAACAG(E21 5A),AAGCCTTTACCAACCATCGCATCAATTAG,GCAAATGCCAGAAAACTAATTG ATGCGA(E256A),CCTGAATTAGCTTTCCAGTTCGAGGATGC,GAAGATACTTAGC CCTGCATCCTCGAACT (K160E), GGTGATTACACTATTGCAAATGCCAGAG,CCAACCATCTCATCAATTAGTGCTCT GGC(K252A),CTATTGCAAATGCCAGAAAACTAATTGCT,CCTTTACCAACCATCT CAGCAATTAGTTT (D255A). Primers for G2A, C3S, R118H, E138G, R211L, R282W have been previously published.

To achieve expression of the constructs in mammalian cells, RP2 coding sequences were transferred into the destination vector pCDNA-DEST40 (Invitrogen), which added an N-terminal V5 tag to the construct, by recombination reaction using LR Clonase II (part of the Invitrogen Gateway cloning system).

Cell culture techniques (motility, transfections, fractionations)

HEK293T, hTERT-RPE1 and HeLa cells were obtained from the ATCC (American type culture collection) and maintained as adherent cultures at 37 ^{o}C and 5% CO_2. HEK293T and HeLa were grown in Dulbecco's modified Eagle medium (DMEM) with 4.5g/l L/D glucose and pyruvate (Gibco, Life Technologies), with the addition of 10% v/v fetal calf serum and penicillin/streptomycin cocktail at 1 mg/ml final concentration. hTERT-RPE1 were grown in DME-F12 medium (Hyclone, Thermo Fisher Scientific) with the addition of 10% v/v fetal calf serum, penicillin/streptomycin cocktail at 1 mg/ml final concentration and hygromycin (10 µg/ml final concentration). Cells were regularly split using the TrypLE trypsin substitute (ThermoFisher Scientific). All cells were routinely tested for contamination by MRC HGU technical services.

Cells were transiently transfected with 0.5 µg purified plasmid DNA containing the relevant constructs (per $0.2x10^6$ cells, using the nonliposomal reagent Fugene HD (Promega).

Cell motility of hTERT-RPE1 cells was assessed by random migration assay and scratch wound assay using the Incucyte ZOOM live-cell imaging system (Essen Bioscience). For the random migration assay, cells were sparsely plated (1,000 cells per well of a 96-well plate), left overnight to adhere and imaged the next day. Distance covered by individual cells was analysed blindly using FiJi software. For the scratch wound assay, cells were plated in 96-well plates and were subjected to a scratch wound when completely confluent (using the WoundMaker tool by Essen Bioscience). Density of cells migrating into the wound during the next 24 hours was measured by the Incucyte cell migration software.

Cell lysate proteins were separated according to three subcellular fractions (cytoplasmic, membrane/organelle and nuclear/cytoskeletal) using a detergent-based cell fractionation kit (Cell Signaling technology) according to manufacturer's instructions.

Antibodies used for western blotting, immunoprecipitation

The following primary antibodies were used for western blotting: mouse monoclonal anti-V5, 1: 5,000 (Life technologies R960-25), rabbit polyclonal anti-OSTF1, 1: 10,000 (Bethyl laboratories A303-004A), mouse monoclonal anti-β actin, 1: 10,000 (Sigma-Aldrich A3853), rabbit polyclonal anti-RP2, 1: 2,000 (custom-made [7]), mouse monoclonal anti-histone H3, 1: 1,000 (Abcam ab18521), rabbit polyclonal anti-Integrin β1, 1:500 (Millipore AB1952), rabbit monoclonal anti-FLAG, 1:2,000 (Cell Signalling #8146), mouse monoclonal anti-c-Cbl, 1:1,000 (BD Bioscience 610441) rabbit polyclonal anti-Myc, 1:1,000 (CST 2278) and rabbit monoclonal anti-pERK, 1:1,000 (CST 4370).

V5 and FLAG IPs were conducted in triton lysis buffer (50mM Tris pH 7.4, 150mM NaCl, 1% Triton-X100). For V5 IPs, 10 µl of anti-V5 agarose affinity gel (Sigma-Aldrich) was incubated with 2-3 mg of total cell lysate protein for 1 hr at 4^{o}C under continuous rotation. For FLAG IPs, 5 µl of EZ View red anti-FLAG M2 agarose affinity gel (Sigma-Aldrich) were incubated with 1 mg of total cell lysate protein for 2 hrs at 4^{o}C under continuous rotation. After incubation, extensive washes followed to minimize non-specific protein binding. In the end, immunocomplexes were eluted off the beads by adding LDS buffer (NuPage, Life technologies)/DTT and subjected to SDS-PAGE and western blotting.

Plasmids and proteins

Native full length ARL3 or truncated ARL3 aa 17-177 (ARL3ΔN), RP2, RP2 aa 250-350 (ΔN), RP2 aa 35-350 (ΔN34) and RP2 mutant R211H were purified as previously described to be completely loaded with GppNHp[3,16]. OSTF1 FL, OSTF1 aa 1-74 (OSTFΔC) and OSTF1 aa 74-214 (ΔN) were cloned into pET20 vector and purified in a three-step procedure via affinity chromatography (self-packed NTA material,

QIAGEN), a hydrophobic phenyl sepharose column (GE Healthcare) and gel filtration using a Superdex 75 16/60 column (GE Healthcare). Buffers were used as previously described[44,45]. The proteins were stored in buffer M containing 25 mM Hepes pH 7.5, 150 mM NaCl, 5 mM $MgCl_2$, 1 mM DTE and 5% glycerol.

GST-ARL3 Q71L, GST-OSTF1 and RP2-GST recombinant proteins used in pulldown experiments were expressed in BL21 DE3 *E.coli* cells transformed with pGEX4T3 vectors (GE Healthcare) containing the relevant constructs. GST-tagged (at the N-terminal or C-terminal in the case of RP2) recombinant proteins were purified from the cell lysate by immobilization on glutathione-sepharose bead slurry (GE Healthcare). The protein-bound slurry was stored in PBS containing 10% glycerol and 1 mM DTT.

Pulldown assays

GST pulldown assays were conducted in mild lysis buffer (25 mM Tris-HCl pH 7.5, 150 mM NaCl, 1 mM EDTA, 1% NP40, 5% glycerol) by incubating 0.7-1 mg of total cell lysate or bovine retinal extract protein with ~10 µg of GST-tagged protein bound on glutathione-sepharose beads for 2 hrs at 4^{o}C under continuous rotation. The bead-bound GST protein complexes were washed at least three times in lysis buffer to remove non-specifically bound proteins. In the end, GST complexes were eluted off the beads by the addition of LDS buffer (NuPage, Life Technologies)/DTT and submitted to SDS-PAGE and western blotting.

Isothermal Titration Calorimetry (ITC) measurements

Interactions of RP2 and RP2 R211H with OSTF FL were investigated by isothermal calorimetry using an ITC_{200} microcalorimeter (MicroCal). Measurements were carried out in buffer M at 25°C. 585 µM OSTF FL protein in the syringe was injected into the cell containing either of 58 µM RP2 or 52 µM RP2 R211H. Analysis of the data was performed using the Origin 7.0 Software provided by the manufacturer (MicroCal, LLC ITC).

Analytical size exclusion chromatography

Complex formation of RP2, RP2ΔN or RP2ΔN34 with OSTF1 FL, OSTFΔN or OSTFΔC was investigated by analytical size exclusion chromatography using a Superdex 75 10/300 column (GE Healthcare). A total of 0.5 mg RP2 protein was incubated with equal molar amounts of OSTF1 protein for 2 hours at room temperature. The mix was then applied to the size exclusion chromatography column and eluted with one column volume of buffer M. The elution profile was recorded and eluted fractions analysed by SDS–PAGE.

Affinity measurements

ARL3ΔN was loaded with mantGDP or mantGppNHp (Pharma Waldhof) overnight at 12°C by incubation with a 1.5 fold molar excess of nucleotide and purified the following day on a desalting column in buffer M[16]. In case of mantGppNHp alkaline phosphatase was added. Nucleotide loading was determined by HPLC measurements on a C18 column. Polarization data was recorded with a Fluoromax-4 spectrophotometer (Jobin Yvon, München, Germany), with excitation and emission wavelengths of mant-nucleotides at 366 and 450 nm, respectively.

Qualitative binding and complex formation of OSTF1 FL with ARL3ΔN was determined by titration of 1 µM ARL3ΔN bound to the respective mant-nucleotide with increasing amounts of OSTF1 FL. For triple complex formation 1 µM ARL3ΔN bound to mantGppNHp was supplemented with 10 µM RP2 followed by 20 µM OSTF1 FL or buffer, respectively.

Binding affinities of RP2 to ARL3ΔN were measured by monitoring the polarization signal during titration of 1 µM ARL3 loaded with mantGppNHp with increasing amounts of RP2 in the presence or absence of 10 µM OSTF1 FL at 20°C in buffer M. Obtained data points were fitted to a first-order reaction using Grafit5 (Erithacus software) to obtain the dissociation constant, K_d.

The affinity of OSTF1 FL to RP2 was determined indirectly by formation of a complex of 1µM ARL3 mantGppNHp with 1µM RP2 which was titrated with increasing amounts of OSTF1 FL at 20°C in buffer M. Obtained data points were fitted to a first-order reaction using Grafit5 (Erithacus software) to obtain the dissociation constant, K_d.

Measurement of GTP hydrolysis by [γ-^{32}P]GTP charcoal method

This was performed as described before[16]. ARL3 was loaded with GppCH$_2$p with the help of bead-linked alkaline phosphatase which was removed via centrifugation and another step of gel filtration. Briefly, a mix of 20 µM ARL3-GppCH$_2$p was mixed with 60 nM [γ-^{32}P]GTP and 18 µM GTP in Buffer M. Upon a short incubation, the reaction was started by addition of 0.2 µM RP2 or 5 µM OSTF1 or a mix of 0.2 µM RP2/5µM OSTF1. Aliquots of 10 µl were taken at 10, 20, 40, 60, 90, 120 180, 240 and 300 seconds and immediately mixed with 400 µl of charcoal solution (50 g*l-1 charcoal in 20 mM phosphoric acid) to stop the reaction. The charcoal was pelleted and the amount of free ^{32}Pi in the supernatant determined by scintillation counting. Data was plotted by showing ratio of specific counts per minute (cpm) of supernatant over total counts per minute of sample at each point.

Structure-based *in silico* analyses

The empirical forcefield FoldX[46,47] under the YASARA[48,49] molecular visualisation program was used to estimate the free energy difference (stability change) upon mutagenesis from wild-type as previously described[17]

In order to retrieve and select a divergent set of RP2 orthologue sequences for multiple sequence alignment, the ConSurf server [50,51] was used with the following options (Homologue search algorithm: CSI-BLAST; Number of iterations: 3; E-value cut-off: 0.0001; Protein database: UniRef-90; Maximal % identity between sequences: 95%; Minimal % identity for homologues: 35%). From the returned results, the set of sequences was further manually curated to exclude all 'fragment' proteins and those proteins that could not be assigned to any genus after cross-checking their UniRef Accession IDs. Thus, eighteen sequences were finally selected and aligned externally using MUSCLE[52]. The alignment was used as input for the ConSurf web server to map sequence conservation on the protein structure of RP2. The 'Bayesian' method was used to calculate the rate of evolution at each site using the 'JTT' evolutionary substitution matrix model. The PyMOL Molecular Graphics System (Schrödinger, LLC.) was used for visualization, analysis and figure preparation.

The electrostatic surface representation of RP2 was generated by GRASP[53] and the lipophilic surface rendition was generated using MOLCAD[54].

Docking model of the RP2-OSTF1 interaction

We used the program HADDOCK[55] using the standard protein-protein docking protocol in order to generate docking models of RP2-OSTF1 dimers from the known structures of RP2 (PDB ID: 3BH7) and OSTF1 (PDB ID: 3EHR). The interaction surface on RP2 was based on the mutagenesis experiments: the four residues that can disrupt the interaction when mutated (Arg211, Lys160, Tyr245 and Asp255) are defined as "active" and were constrained to be directly involved in the interface, whereas other surface residues within 8 Å of these residues were defined as "passive" and were allowed but not strictly constrained to participate in the interface. However, since we do not know what residues from OSTF1 directly interact, we

performed a series of docking runs where the OSTF1 interface was constrained to be centred around each of the 121 surface residues (defined as exposing >20 Å of solvent-accessible surface area). Surface residues within 3 Å of the central residues are defined as core, while other residues within 8 Å are defined as passive.

Initially, we generated 55 water-refined docking models for each OSTF1 surface residue. For each docking model, we used FoldX to predict the effects of each experimentally tested mutation on the RP2-OSTF1 interaction. Next, we identified docking models that meet the following criteria: i) the interaction involves both the N-domain (residues 13-73) and C-terminal domain (residues 74-190); ii) the OSTF1 binding surface does not overlap with the known SH3 binding pocket (residues 21-24, 26-30, 35, 46-49, 60, 62, 64-65, 68-69); iii) no steric clashes between OSTF1 and ARL3; and iv) *P*-value < 0.05 for a Wilcoxon rank-sum test comparison between the predicted FoldX effects of the disruptive mutations (R211L, K160A, K160E, Y245A, D255A) *vs* non-disruptive mutations (R118H, E138G, R282W, E205A, E206A, K208A, S213A, E215A, R218S, K252A, E256A). For the 73 OSTF1 surface residues that had at least one structure compatible with these criteria, we generated 100 additional docking models. We then further identified docking models that meet the above criteria, except they have a *P*-value < 0.002. For the 53 OSTF1 surface residues that had at least one structure compatible with these criteria, we generated 200 additional docking models.

Out of the 24555 docking models generated in total, there were 21 that met the above criteria, but also had HADDOCK scores < -50, and in which the predicted effects of all disruptive mutations are stronger than all non-disruptive mutations. These 21 structures were then clustered on the basis of their C□C□ root-mean-square deviation (RMSD), with all structures in each cluster having <3 Å RMSD with all others.

To assess the evolutionary conservation of OSTF1 interaction surfaces from each docking model, we used the residue-specific values calculated by ConSurf[29] and then calculated the average value for interface-forming residues, normalised by the amount of surface area per residue buried in the interface.

Acknowledgements

T.H. is funded by the MRC Human Genetics Unit and a University of Edinburgh Chancellor's fellowship. This work was supported by grant funding [GR588] from RP Fighting Blindness (www.rpfightingblindness.org.uk).

This work was supported by ERC grant ARCID268782 to A.W.

R.L. is supported by an MRC/University of Edinburgh PhD studentship grant.

J.M. is supported by a Medical Research Council Career Development Award (MR/M02122X/1).

Contributions

RL and ML performed most experiments and RL wrote the manuscript. DS conducted the structure-based *in silico* analyses. JM generated docking models of the RP2-OSTF1 interaction. AW and ML performed preliminary experiments relevant to the project. AW supervised the work and advised on the design. TH supervised the work, designed the experiments and performed experiments.

References

1. Pelletier, V. et al. Comprehensive survey of mutations in RP2 and RPGR in patients affected with distinct retinal dystrophies: genotype-phenotype correlations and impact on genetic counseling. *Hum Mutat* **28**, 81-91 (2007).
2. Prokisch, H., Hartig, M., Hellinger, R., Meitinger, T. & Rosenberg, T. A population-based epidemiological and genetic study of X-linked retinitis pigmentosa. *Invest Ophthalmol Vis Sci* **48**, 4012-8 (2007).
3. Kuhnel, K., Veltel, S., Schlichting, I. & Wittinghofer, A. Crystal structure of the human retinitis pigmentosa 2 protein and its interaction with Arl3. *Structure* **14**, 367-78 (2006).
4. Chapple, J.P. et al. Mutations in the N-terminus of the X-linked retinitis pigmentosa protein RP2 interfere with the normal targeting of the protein to the plasma membrane. *Hum Mol Genet* **9**, 1919-26 (2000).
5. Chapple, J.P., Hardcastle, A.J., Grayson, C., Willison, K.R. & Cheetham, M.E. Delineation of the plasma membrane targeting domain of the X-linked retinitis pigmentosa protein RP2. *Invest Ophthalmol Vis Sci* **43**, 2015-20 (2002).
6. Rosenberg, T., Schwahn, U., Feil, S. & Berger, W. Genotype-phenotype correlation in X-linked retinitis pigmentosa 2 (RP2). *Ophthalmic Genet* **20**, 161-72 (1999).
7. Hurd, T. et al. The retinitis pigmentosa protein RP2 interacts with polycystin 2 and regulates cilia-mediated vertebrate development. *Hum Mol Genet* **19**, 4330-44 (2010).
8. Evans, R.J. et al. The retinitis pigmentosa protein RP2 links pericentriolar vesicle transport between the Golgi and the primary cilium. *Hum Mol Genet* **19**, 1358-67 (2010).
9. Gotthardt, K. et al. A G-protein activation cascade from Arl13B to Arl3 and implications for ciliary targeting of lipidated proteins. *Elife* **4**(2015).
10. Kim, H. et al. Ciliary membrane proteins traffic through the Golgi via a Rabep1/GGA1/Arl3-dependent mechanism. *Nat Commun* **5**, 5482 (2014).
11. Wright, Z.C. et al. ARL3 regulates trafficking of prenylated phototransduction proteins to the rod outer segment. *Hum Mol Genet* **25**, 2031-2044 (2016).
12. Ismail, S.A. et al. Arl2-GTP and Arl3-GTP regulate a GDI-like transport system for farnesylated cargo. *Nat Chem Biol* **7**, 942-9 (2011).
13. Ismail, S.A. et al. Structural basis for Arl3-specific release of myristoylated ciliary cargo from UNC119. *Embo j* **31**, 4085-94 (2012).
14. Schrick, J.J., Vogel, P., Abuin, A., Hampton, B. & Rice, D.S. ADP-ribosylation factor-like 3 is involved in kidney and photoreceptor development. *Am J Pathol* **168**, 1288-98 (2006).
15. Hanke-Gogokhia, C. et al. Arf-like Protein 3 (ARL3) Regulates Protein Trafficking and Ciliogenesis in Mouse Photoreceptors. *J Biol Chem* **291**, 7142-55 (2016).
16. Veltel, S., Gasper, R., Eisenacher, E. & Wittinghofer, A. The retinitis pigmentosa 2 gene product is a GTPase-activating protein for Arf-like 3. *Nat Struct Mol Biol* **15**, 373-80 (2008).
17. Liu, F. et al. Pathogenic Mutations in Retinitis Pigmentosa 2 Predominantly Result in Loss of RP2 Protein Stability in Human and Zebrafish. *J Biol Chem* (2017).

18. Strom, S.P. et al. De Novo Occurrence of a Variant in ARL3 and Apparent Autosomal Dominant Transmission of Retinitis Pigmentosa. *PLoS One* **11**, e0150944 (2016).
19. Zhang, H. et al. Mistrafficking of prenylated proteins causes retinitis pigmentosa 2. *Faseb j* **29**, 932-42 (2015).
20. Li, L. et al. Ablation of the X-linked retinitis pigmentosa 2 (Rp2) gene in mice results in opsin mislocalization and photoreceptor degeneration. *Invest Ophthalmol Vis Sci* **54**, 4503-11 (2013).
21. Togi, S. et al. A New STAT3-binding Partner, ARL3, Enhances the Phosphorylation and Nuclear Accumulation of STAT3. *J Biol Chem* **291**, 11161-71 (2016).
22. Yoon, J.H. et al. The retinitis pigmentosa-mutated RP2 protein exhibits exonuclease activity and translocates to the nucleus in response to DNA damage. *Exp Cell Res* **312**, 1323-34 (2006).
23. Reddy, S. et al. Isolation and characterization of a cDNA clone encoding a novel peptide (OSF) that enhances osteoclast formation and bone resorption. *Journal of Cellular Physiology* **177**, 636-645 (1998).
24. Szymkiewicz, I., Destaing, O., Jurdic, P. & Dikic, I. SH3P2 in complex with Cbl and Src. *FEBS Lett* **565**, 33-8 (2004).
25. Tanimura, S. et al. SH3P2 is a negative regulator of cell motility whose function is inhibited by ribosomal S6 kinase-mediated phosphorylation. *Genes Cells* **16**, 514-26 (2011).
26. Tanimura, S. et al. ERK signaling promotes cell motility by inducing the localization of myosin 1E to lamellipodial tips. (2016).
27. Thiselton, D.L. et al. Novel frameshift mutations in the RP2 gene and polymorphic variants. *Hum Mutat* **15**, 580 (2000).
28. Miano, M.G. et al. Identification of novel RP2 mutations in a subset of X-linked retinitis pigmentosa families and prediction of new domains. *Hum Mutat* **18**, 109-19 (2001).
29. Ashkenazy, H. et al. ConSurf 2016: an improved methodology to estimate and visualize evolutionary conservation in macromolecules. *Nucleic Acids Res* **44**, W344-50 (2016).
30. Huttlin, E.L. et al. The BioPlex Network: A Systematic Exploration of the Human Interactome. *Cell* **162**, 425-40 (2015).
31. Kurihara, N., Menaa, C., Maeda, H., Haile, D.J. & Reddy, S.V. Osteoclast-stimulating factor interacts with the spinal muscular atrophy gene product to stimulate osteoclast formation. *J Biol Chem* **276**, 41035-9 (2001).
32. Tanimura, S. et al. Activation of the 41/43 kDa mitogen-activated protein kinase signaling pathway is required for hepatocyte growth factor-induced cell scattering. *Oncogene* **17**, 57-65 (1998).
33. McConnell, R.E. & Tyska, M.J. Leveraging the membrane - cytoskeleton interface with myosin-1. *Trends Cell Biol* **20**, 418-26 (2010).
34. Krendel, M. et al. Disruption of Myosin 1e promotes podocyte injury. *J Am Soc Nephrol* **20**, 86-94 (2009).
35. Ouderkirk-Pecone, J.L. et al. Myosin 1e promotes breast cancer malignancy by enhancing tumor cell proliferation and stimulating tumor cell de-differentiation. *Oncotarget* **7**, 46419-46432 (2016).

36. Cheng, J., Grassart, A. & Drubin, D.G. Myosin 1E coordinates actin assembly and cargo trafficking during clathrin-mediated endocytosis. *Mol Biol Cell* **23**, 2891-904 (2012).
37. Megaw, R. et al. Gelsolin dysfunction causes photoreceptor loss in induced pluripotent cell and animal retinitis pigmentosa models. *Nat Commun* **8**, 271 (2017).
38. Ruiz-Loredo, A.Y. & Lopez-Colome, A.M. New insights into the regulation of myosin light chain phosphorylation in retinal pigment epithelial cells. *Int Rev Cell Mol Biol* **293**, 85-121 (2012).
39. Higginbotham, H. et al. Arl13b in primary cilia regulates the migration and placement of interneurons in the developing cerebral cortex. *Dev Cell* **23**, 925-38 (2012).
40. Lyraki, R., Megaw, R. & Hurd, T. Disease mechanisms of X-linked retinitis pigmentosa due to RP2 and RPGR mutations. *Biochem Soc Trans* **44**, 1235-1244 (2016).
41. Jayasundera, T. et al. THE RP2 PHENOTYPE AND PATHOGENETIC CORRELATIONS IN X-LINKED RETINITIS PIGMENTOSA. *Arch Ophthalmol* **128**, 915-23 (2010).
42. Pierce, E.A. & Bennett, J. The Status of RPE65 Gene Therapy Trials: Safety and Efficacy. *Cold Spring Harb Perspect Med* **5**, a017285 (2015).
43. Mookherjee, S. et al. Long-term rescue of cone photoreceptor degeneration in retinitis pigmentosa 2 (RP2)-knockout mice by gene replacement therapy. *Hum Mol Genet* **24**, 6446-58 (2015).
44. Chen, L. et al. Structure of the SH3 domain of human osteoclast-stimulating factor at atomic resolution. *Acta Crystallogr Sect F Struct Biol Cryst Commun* **62**, 844-8 (2006).
45. Tong, S. et al. Crystal structure of human osteoclast stimulating factor. *Proteins: Structure, Function, and Bioinformatics* **75**, 245-251 (2016).
46. Schymkowitz, J. et al. The FoldX web server: an online force field. *Nucleic Acids Res* **33**, W382-8 (2005).
47. Guerois, R., Nielsen, J.E. & Serrano, L. Predicting changes in the stability of proteins and protein complexes: a study of more than 1000 mutations. *J Mol Biol* **320**, 369-87 (2002).
48. Van Durme, J. et al. A graphical interface for the FoldX forcefield. *Bioinformatics* **27**, 1711-2 (2011).
49. Krieger, E., Koraimann, G. & Vriend, G. Increasing the precision of comparative models with YASARA NOVA--a self-parameterizing force field. *Proteins* **47**, 393-402 (2002).
50. Glaser, F. et al. ConSurf: identification of functional regions in proteins by surface-mapping of phylogenetic information. *Bioinformatics* **19**, 163-4 (2003).
51. Ashkenazy, H., Erez, E., Martz, E., Pupko, T. & Ben-Tal, N. ConSurf 2010: calculating evolutionary conservation in sequence and structure of proteins and nucleic acids. *Nucleic Acids Res* **38**, W529-33 (2010).
52. Edgar, R.C. MUSCLE: a multiple sequence alignment method with reduced time and space complexity. *BMC Bioinformatics* **5**, 113 (2004).
53. Nicholls, A., Sharp, K.A. & Honig, B. Protein folding and association: insights from the interfacial and thermodynamic properties of hydrocarbons. *Proteins* **11**, 281-96 (1991).
54. Heiden, W., Moeckel, G. & Brickmann, J. A new approach to analysis and display of local lipophilicity/hydrophilicity mapped on molecular surfaces. *J Comput Aided Mol Des* **7**, 503-14 (1993).

55. Dominguez, C., Boelens, R. & Bonvin, A.M. HADDOCK: a protein-protein docking approach based on biochemical or biophysical information. *J Am Chem Soc* **125**, 1731-7 (2003).

Figures

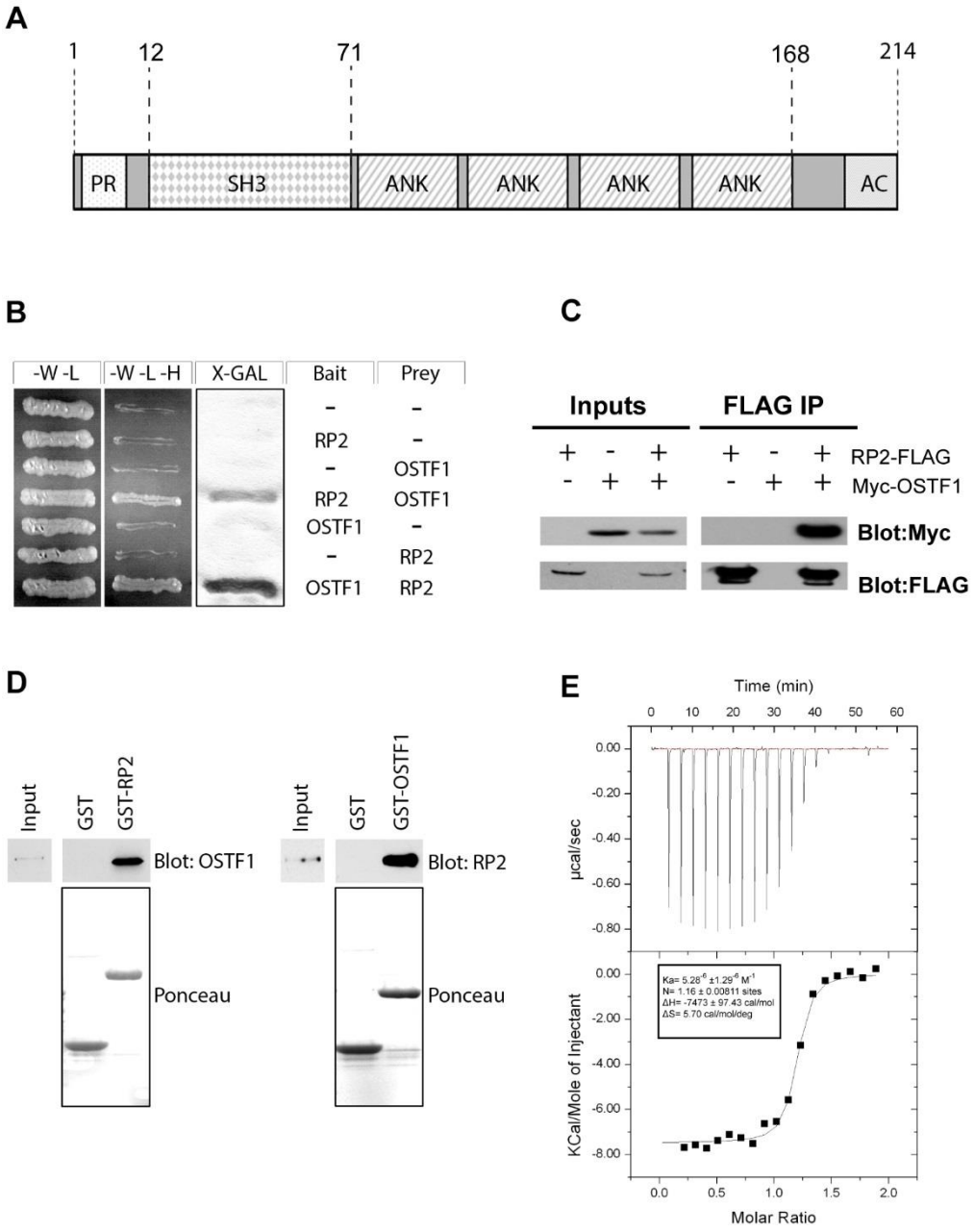

Figure 1. RP2 directly interacts with OSTF1. a) Schematic showing the main protein domains of OSTF1. PR: proline-rich region, SH3: Src-homology 3 domain, ANK: ankyrin repeats, AC: acidic amino acid cluster. b) Direct interaction between RP2 and OSTF1 was identified in a yeast two-hybrid screen and confirmed in two directions in a targeted yeast two-hybrid assay. c) Exogenous RP2 and OSTF1 co-precipitate from HEK293T lysates. Lysates from HEK293T cells previously

transfected with plasmids containing RP2-FLAG and/or Myc-OSTF1 were subjected to anti-FLAG immunoprecipitation (IP) followed by immunoblotting with anti-Myc or anti-FLAG antibodies. d) Bovine retinal extracts were subjected to pull-down assays using recombinant GST-RP2 or GST-OSTF1 as bait, followed by immunoblot for endogenous OSTF1 or RP2, respectively. Ponceau staining shows the GST-tagged proteins. e) Thermodynamic characterisation of the OSTF1-RP2 interaction by isothermal titration calorimetry. 0.585 mM His-tagged OSTF1 were injected into 52 μM full-length RP2 in the sample cell.

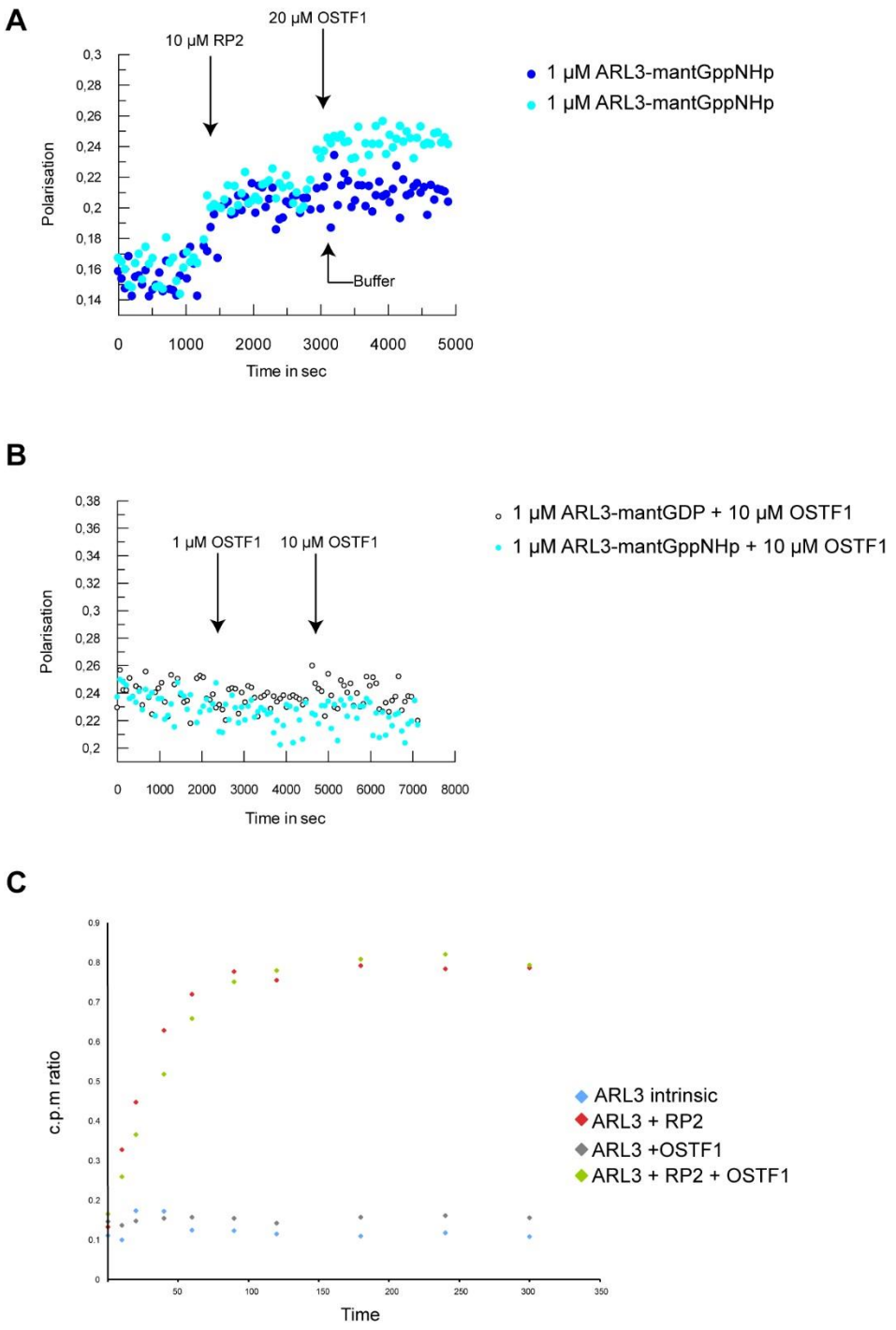

Figure 2. Binding of OSTF1 on RP2 does not affect the RP2-ARL3 interaction. a,b) Complex formation between recombinant OSTF1-His, RP2 and ARL3 (a), as well as between recombinant OSTF1-His and ARL3 (b), was monitored on the basis of change in fluorescence polarisation signal. The fluorescently-labelled G domain of ARL3 was used in the analysis in the following states: mantGppNHp (a non-hydrolysable GTP analog) -bound ARL3 and mantGDP -bound ARL3. c) Binding to OSTF1 does not affect the catalytic activity of RP2. GTPase charcoal assay was

performed with catalytic concentrations of RP2 (GAP) (0.2 μM) and ARL3 (small G protein) (20 μM) bound to 60 nM [^{32}P-γ]GTP, in the presence or absence of 5 μM of OSTF1. GTP hydrolysis is presented as the ratio of counts at each time-point and total counts (c.p.m ratio) over time.

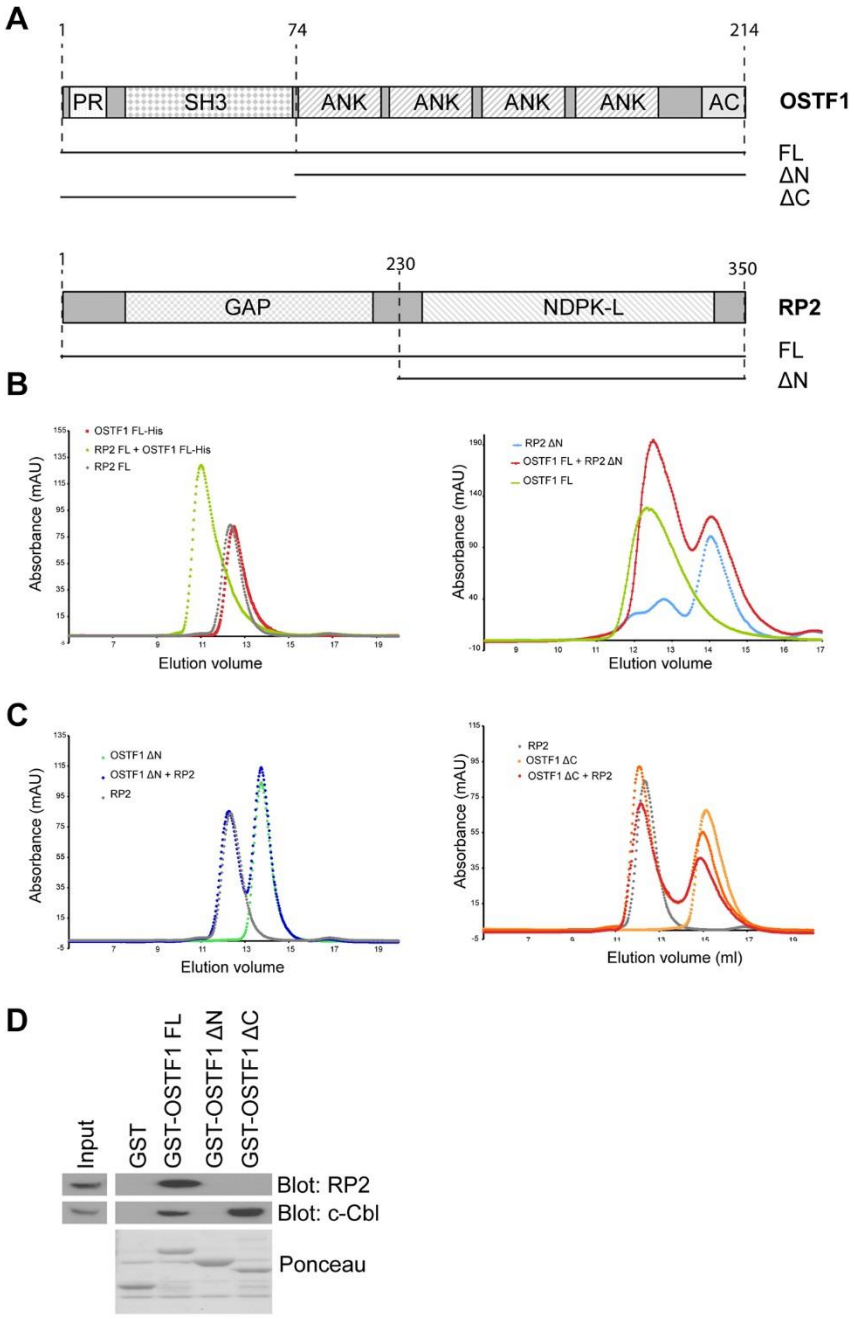

Figure 3. The N- terminal domain of RP2 and both the SH3 and ANK domains of OSTF1 participate in the interaction. a) Diagram of the deletion constructs of OSTF1-His and RP2 that were used in the analytical gel filtration and pull-down assays. RP2 ΔN corresponds to residues 230-350, while OSTF1 ΔN corresponds to residues 75-214 and OSTF1 ΔC to residues 1-73. b) Analytical gel filtration graphs showing complex formation or not between recombinant full-length OSTF1-His and either full-length RP2 (left) or RP2 ΔN (right). c) Analytical gel filtration graphs showing complex formation between recombinant full-length RP2 and either OSTF1 ΔN (left) or OSTF1 ΔC (right). d) To confirm the participation of both OSTF1 domains in the

interaction with RP2, bovine retinal lysates were subjected to pull-down assays using recombinant GST-OSTF1 as bait, either full-length or truncated as indicated, followed by immunoblotting for endogenous RP2 and c-Cbl. Ponceau staining shows the GST-tagged protein.

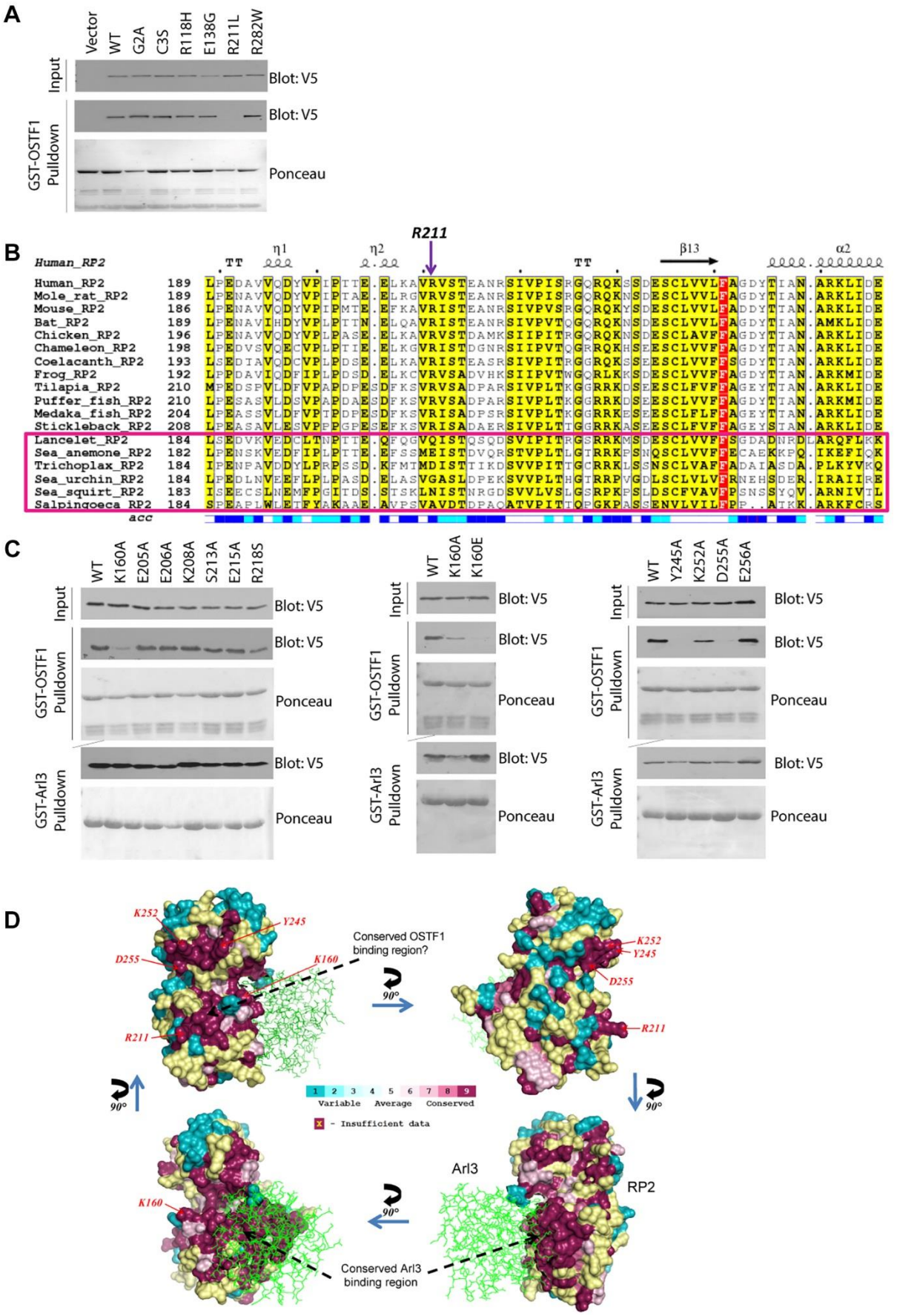

Figure 4. a) The RP2-OSTF1 interaction is abolished by the R211L mutation, contrary to other missense pathogenic mutations. HEK293T cell lysates previously transfected with plasmids containing wild-type RP2-V5 or pathogenic mutant forms of the protein were subjected to pull-down assays using recombinant GST-OSTF1 as bait. Subsequently, they were subjected to immunoblotting using an antibody to V5 tag. Ponceau staining shows the presence of the GST-tagged protein. b) Section of the multiple sequence alignment of RP2 protein orthologues, encompassing the critical OSTF1 interaction position (R211) which is strictly conserved among vertebrates. Non-vertebrate chordates and other phyla are shown within the pink border. An interesting strictly conserved residue in all species tested is highlighted in red (F241 in human RP2). c) Identification of RP2 residues that are critical for the RP2-OSTF1 interaction to occur. HEK293T cell lysates previously transfected with plasmids containing wild-type RP2-V5 or the same protein encompassing non-destabilizing missense mutations were subjected to pull-down assays using recombinant GST-OSTF1 or GST-ARL3 Q71L as bait. ARL3 Q71L mutant is defective in GTP hydrolysis and thus can bind RP2 stably. They were then analysed by immunoblotting using an antibody to V5 tag. Ponceau staining shows the presence of the GST-tagged protein. d) The ARL3 binding area on RP2, as well as the residues that we identified as important for the RP2-OSTF1 interaction (highlighted in red), belong to distinct strictly conserved clusters. The RP2-ARL3 complex crystal structure (PDB ID: 3BH7) is shown in four views rotated by 90^{o} about the y-axis with the ConSurf [50,51]analysis. RP2 is shown in surface representation, where residues are color-coded according to their conservation grade in vertebrates, with turquoise-through-maroon indicating variable to strictly conserved. Light yellow colour represents positions for which the inferred conservation level was assigned with low confidence. ARL3 GTPase is shown in green colour, stick representation.

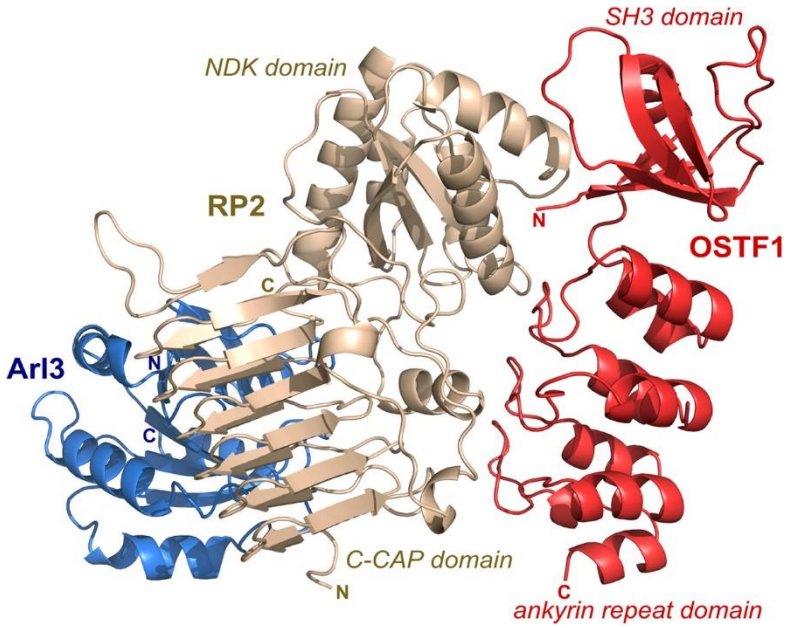

Figure 5. Docking model of the ternary OSTF-RP2-ARL3 complex compatible with experimental mutagenesis data. Shown here is a single structure from Cluster 1 (Supplementary Figure 4), which comprised approximately half of all docking models compatible with the experimental data, and which showed a much more strongly conserved binding surface on OSTF1 than the others.

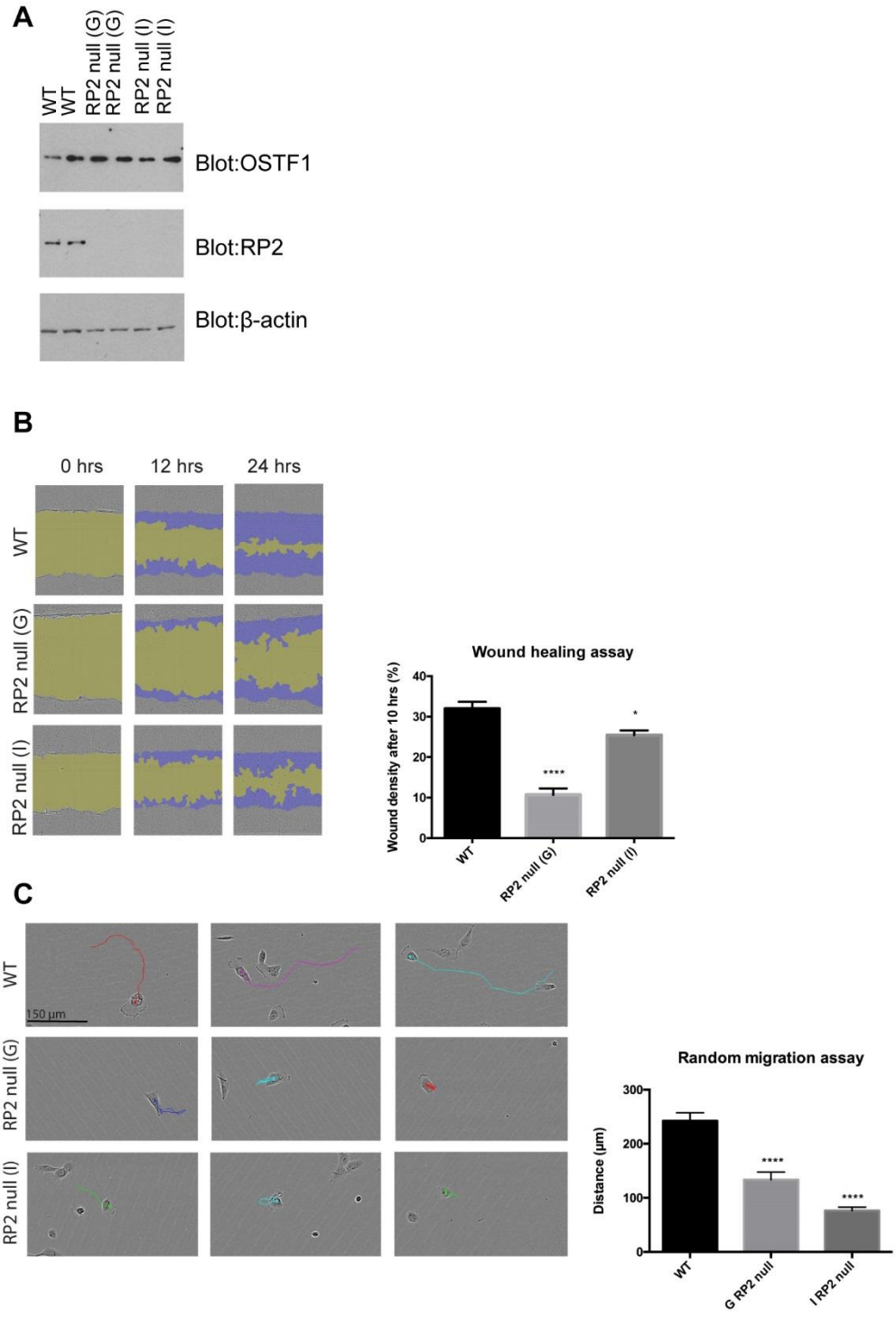

Figure 6. Cells lacking RP2 expression display motility defects a) hTERT-RPE1 cell lines were engineered to be *RP2* null but express OSTF1 at WT levels. Wild-type and *RP2* null hTERT-RPE1 cell lysates (G and I clones, x2 biological repeats) were subjected to immunoblotting using antibodies for endogenous OSTF1, RP2 and β-actin as a loading control. b) Wild-type and *RP2* null hTERT-RPE1 cells (G and I clones) were subjected to a wound healing assay. Images on the left show the state of the wound in two representative time points after wound induction (0 hrs). Yellow

colour represents the wound area, while purple colour at the cell boundaries shows the area that has been covered by migrating cells. The graph on the right shows the area of the wound that was covered by migrating cells 10 hrs after wound induction (mean +/- SEM for 6 technical repeats. $p=0.0103$ for I vs WT, $p<0.0001$ for G vs WT as calculated by two-tailed unpaired t-tests). c) Random migration of sparsely plated individual wild-type and *RP2* null hTERT-RPE1 cells (G and I clones) was analysed over a 9-hr period. Left panels show representative tracks followed by individual cells. The graph on the right shows average distance covered by individual cells (n=40 for each cell line) in µm (mean +/- SEM for 4 technical repeats, $p<0.0001$ for G vs WT, $p<0.0001$ for I vs WT as calculated by two-tailed t-test and two-tailed t-test with Welch's correction, respectively).

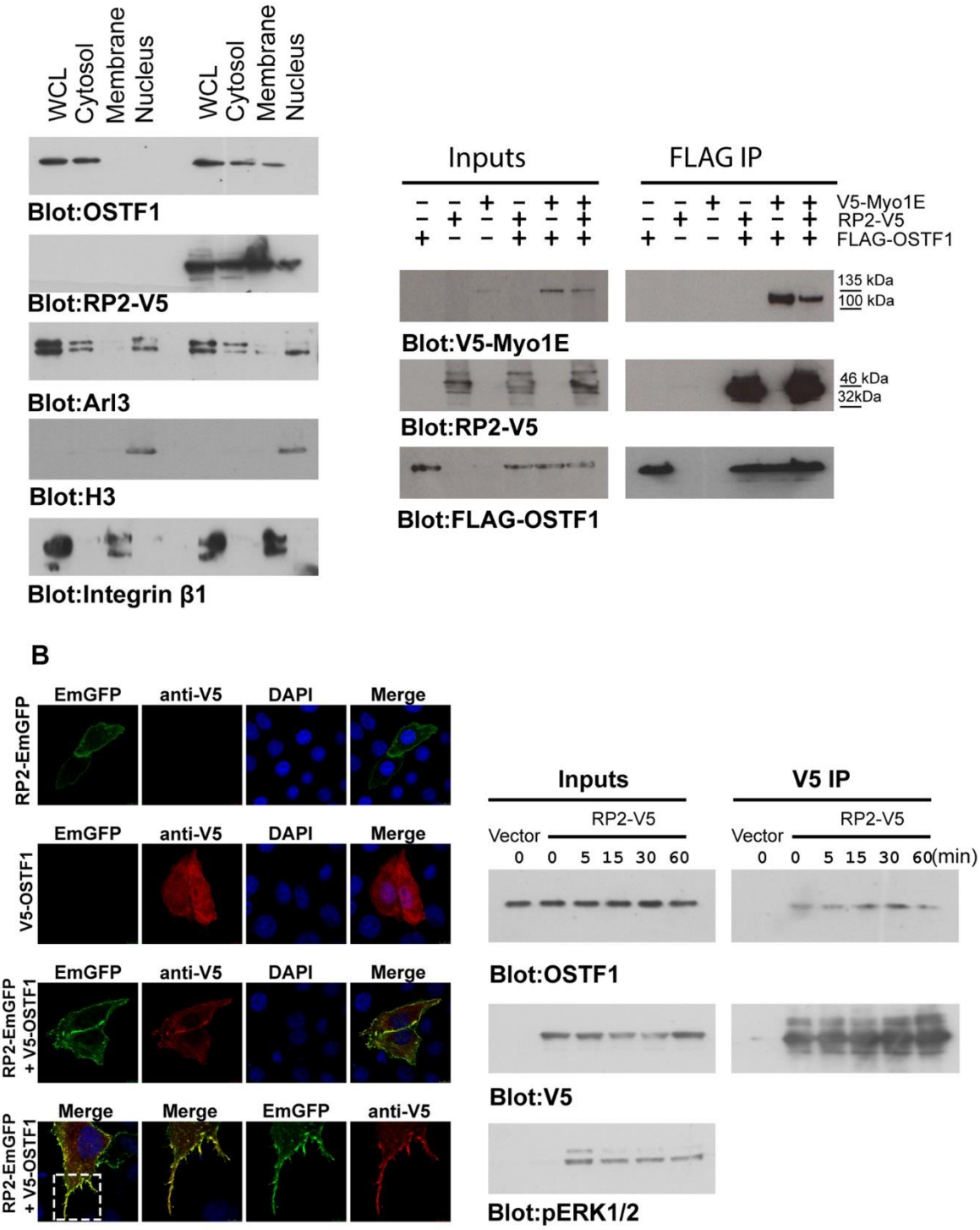

Figure 7. RP2 overexpression leads to OSTF1 translocation to the membrane compartment and dissociation from Myo1E. a) HEK293T cells previously transfected with empty plasmid or plasmid containing an RP2-V5 construct were subjected to detergent-based subcellular fractionation. The fractions were then analysed by immunoblotting using antibodies against V5 tag, endogenous OSTF1, endogenous ARL3, endogenous histone H3 (marker for the nuclear fraction), endogenous integrin β1 (marker for the membrane fraction). While RP2 overexpression led to a

redistribution of OSTF1 pools to the membrane compartment, it did not affect the localisation of ARL3. WCL: whole cell lysate, CF: cytoplasmic fraction, MOF: membrane and organelle fraction, CyNF: cytoplasmic and nuclear fraction. b) HeLa cells previously transfected with plasmids containing RP2-emGFP and/or V5-OSTF1 constructs were fixed and subjected to immunofluorescence using an antibody to V5 tag in order to investigate the localisation of V5-OSTF1. While V5-OSTF1 is cytosolic on its own, RP2 overexpression leads to recruitment of V5-OSTF1 to the plasma membrane. c) HEK293T cells were transiently transfected with plasmids containing different combinations of V5-Myo1E, RP2-V5 and FLAG-OSTF1 constructs. The lysates were subjected to anti-FLAG IP to assess how much V5-Myo1E associated with FLAG-OSTF1 in the presence or absence of RP2-V5 overexpression, and immunoblotting using antibodies to V5 and FLAG tags. d) Stimulation of the ERK1/2 pathway by serum stimulation slightly stabilizes the RP2-OSTF1 interaction. Cells previously transiently transfected with a vector containing an RP2-V5 construct were stimulated with 10% fetal bovine serum for the indicated time duration (in minutes) following overnight serum deprivation. The lysates were then subjected to anti-V5 immunoprecipitation and immunoblotting using antibodies to V5 tag, endogenous OSTF1 and endogenous phospho-ERK1/2.

Supplementary figures

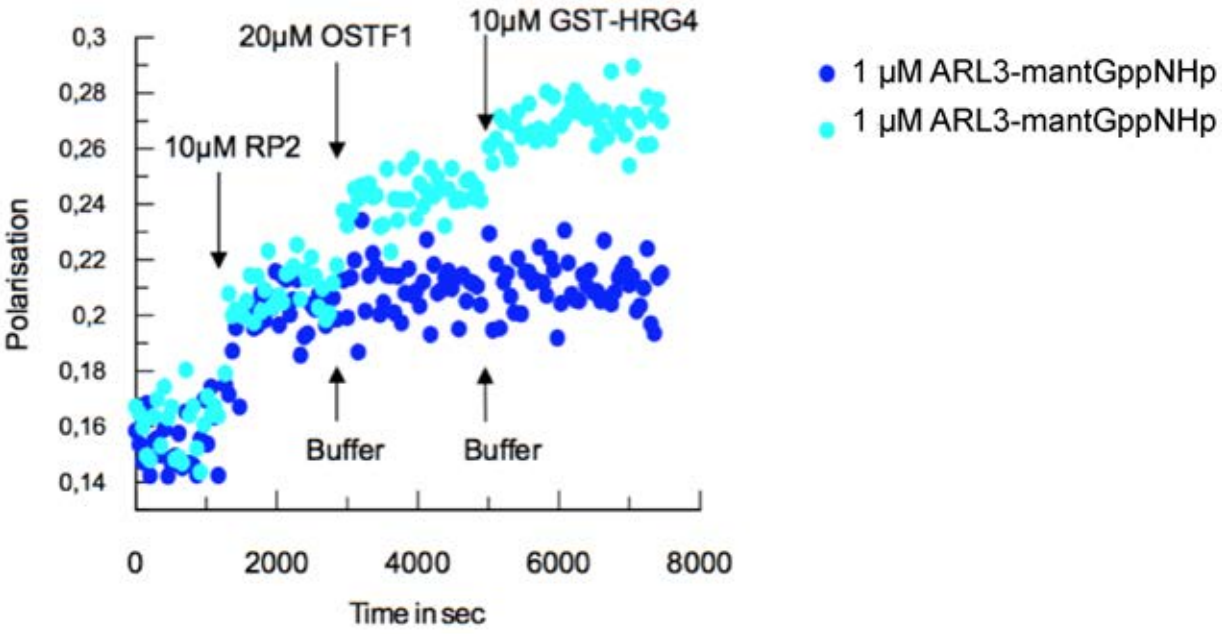

Supplementary Figure 1. The formation of a tetrameric complex between RP2, OSTF1, ARL3 and UNC119a (HRG4) is possible. Complex formation between recombinant OSTF1-His, RP2, GST-HRG4 and fluorescently-labelled G domain of ARL3-mantGppNHp was monitored on the basis of the change in fluorescence polarisation signal.

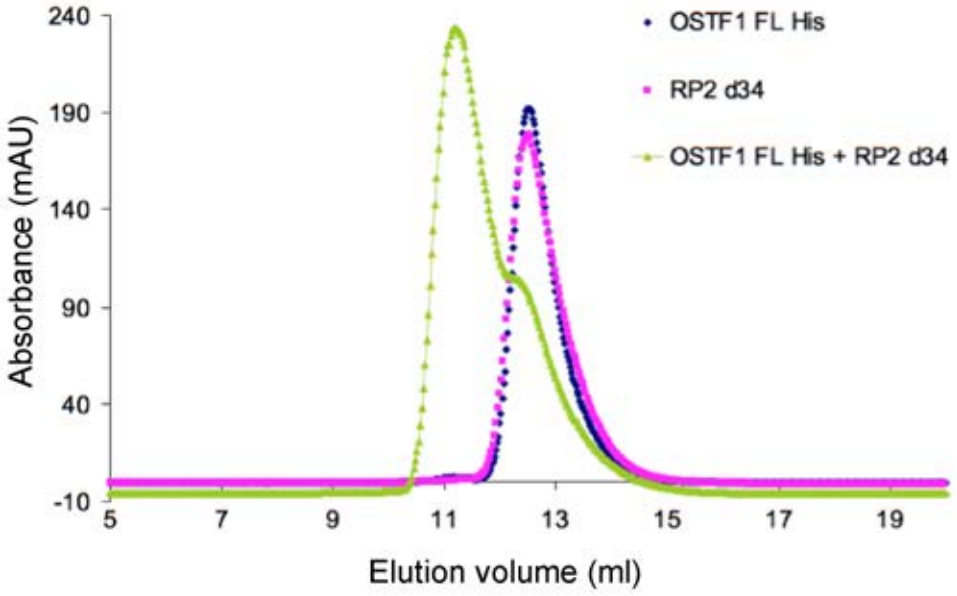

Supplementary Figure 2. The participation of the extreme N-terminus of RP2 is not required for the RP2-OSTF1 interaction to occur. Analytical gel filtration graph showing complex formation between recombinant full-length OSTF1-His and either full-length RP2 or a truncated RP2 protein lacking the first N-terminal 34 residues.

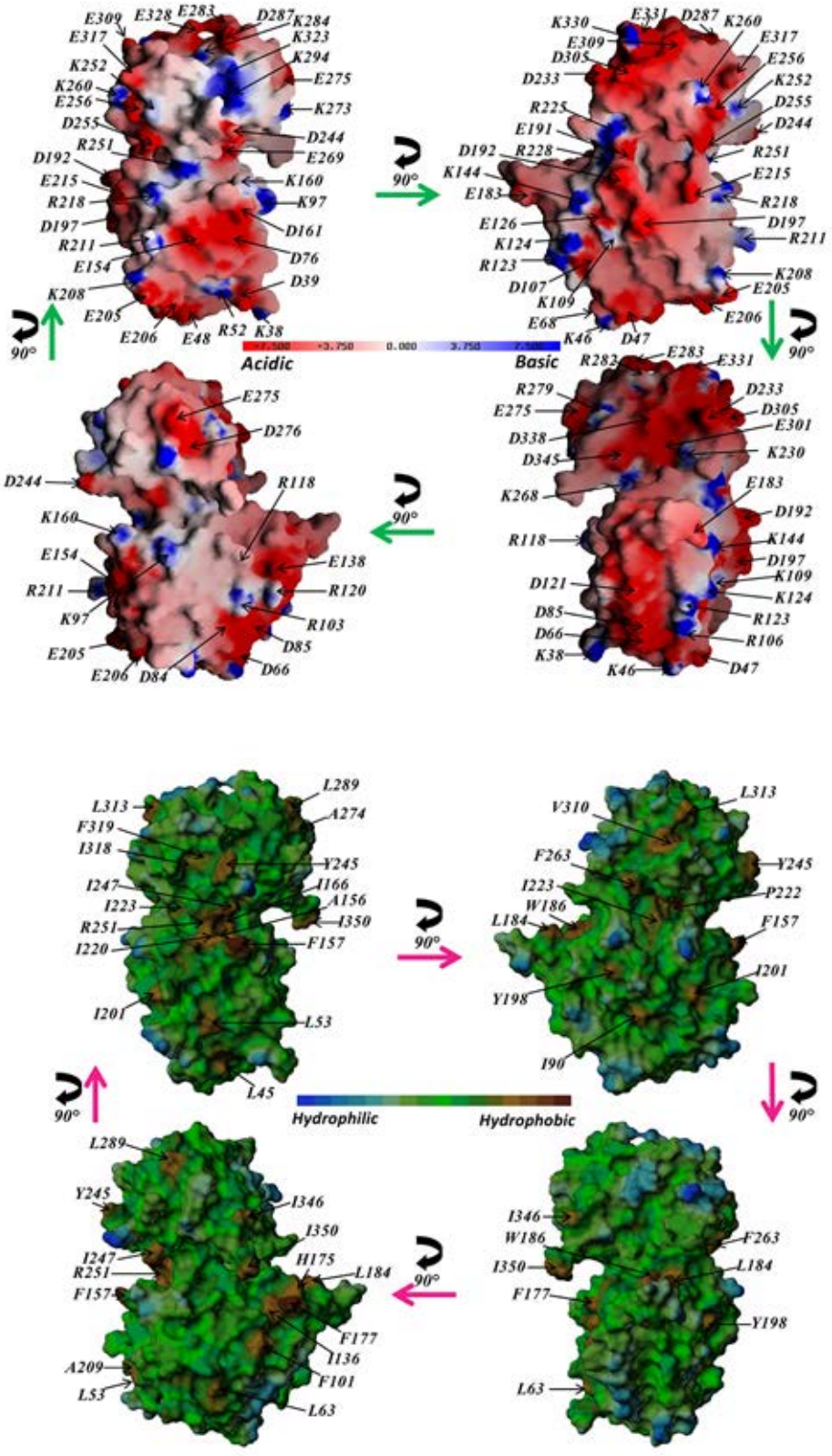

Supplementary figure 3. Lipophilic and electrostatic surface representation of RP2. At the top panel, the RP2 crystal structure (PDB ID: 3BH7) is shown in four views rotating by 90º about the y-axis of a GRASP [53] electrostatic surface representation. Surface charge is color-coded from red (negative) to blue (positive), ranging from -7.5 kT to +7.5 kT (k=Boltzmann's constant; T= temperature in Kelvin). At the bottom panel, the RP2 crystal structure is shown in four views by 90º about the y-axis of a MOLCAD[54] lipophilic surface representation, where exposed regions of high hydrophobicity are coloured brown and regions of high hydrophilicity are coloured blue. The surface representations are in equivalent orientations in the two panels as well as in main figure 4d.

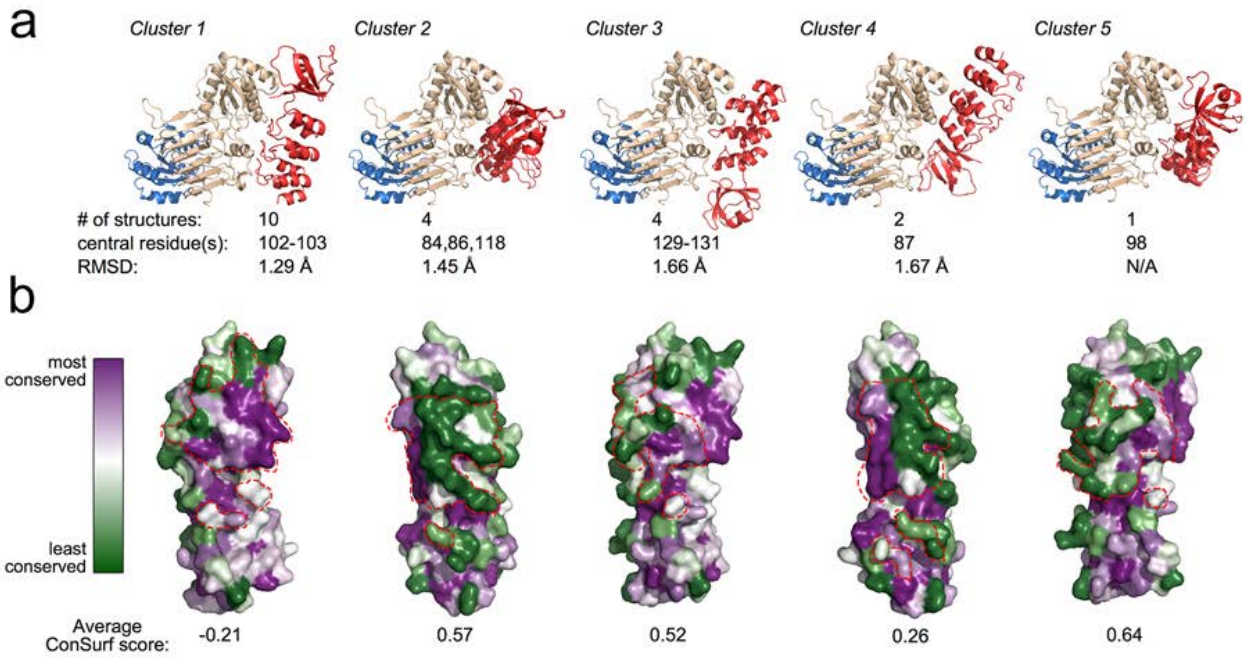

Supplementary figure 4. Five clusters of docking RP2-OSTF1 docking models. All 21 RP2-OSTF1 docking models compatible with the experimental data could be split into five clusters of conformationally similar models. (a) Example of one structure from each cluster, along with the average C□C□ RMSD between all models in the cluster. The central residues indicate those on OSTF1 for which the docking was centred around. (b) Evolutionary conservation scores from ConSurf mapped on the surface of OSTF1, with the binding region of each cluster highlighted. Cluster 1 has a much more conserved binding surface than any of the others.

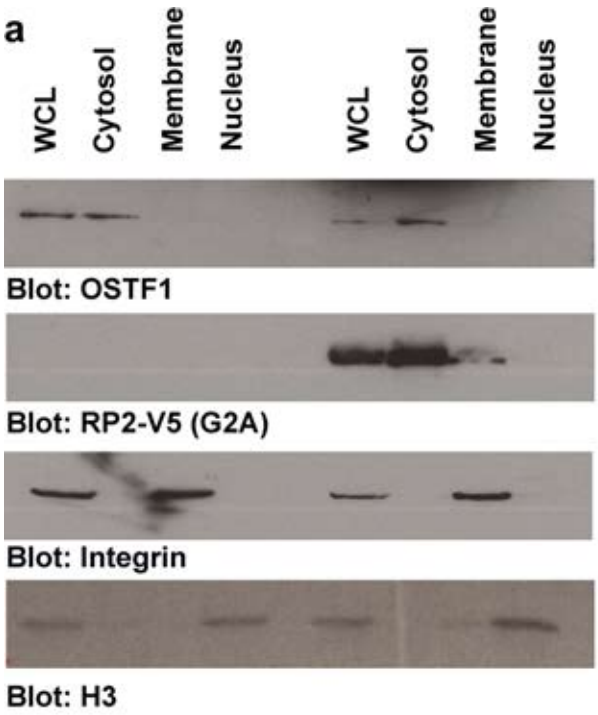

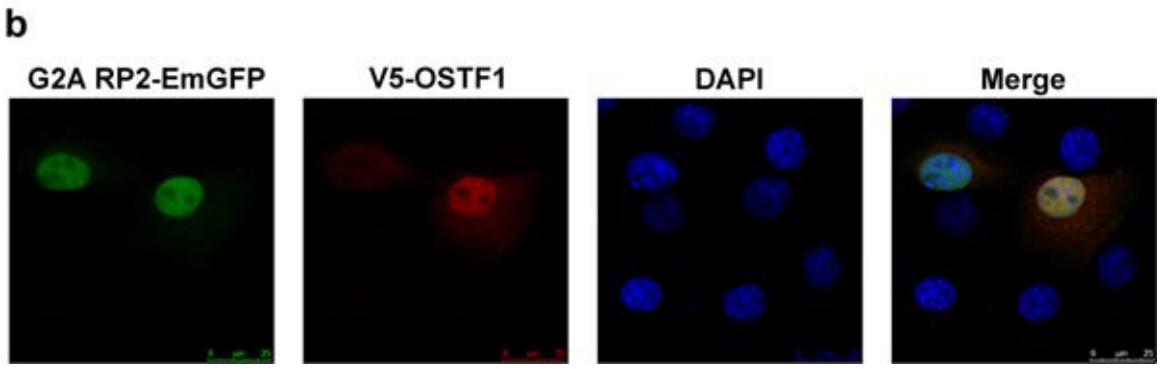

Supplementary figure 5. Overexpression of the membrane targeting-deficient RP2 mutant G2A does not lead to recruitment of OSTF1 to the membrane compartment. a) HEK293T cells previously transfected with empty plasmid or plasmid containing an RP2-V5 construct were subjected to detergent-based subcellular fractionation. The fractions were then analysed by immunoblotting using antibodies against V5 tag, endogenous OSTF1, endogenous histone H3 (marker for the nuclear fraction), endogenous integrin β1 (marker for the membrane fraction). Contrary to the wild-type protein (Figure 7a), RP2 G2A is not enriched in the membrane fraction. Moreover, RP2 G2A overexpression does not lead to a redistribution of OSTF1 to the membrane fraction. WCL: whole cell lysate, CF: cytoplasmic fraction, MOF: membrane and organelle fraction, CyNF: cytoplasmic and nuclear fraction. b) HeLa cells previously transfected with plasmids containing RP2 G2A-emGFP and V5-OSTF1 constructs were fixed and subjected to immunofluorescence using an antibody to V5 tag in order to investigate the localisation of V5-OSTF1. Co-expression of RP2 G2A and OSTF1 does not lead to recruitment of OSTF1 to the plasma membrane, as is the case with the wild-type RP2 (Figure 7a).

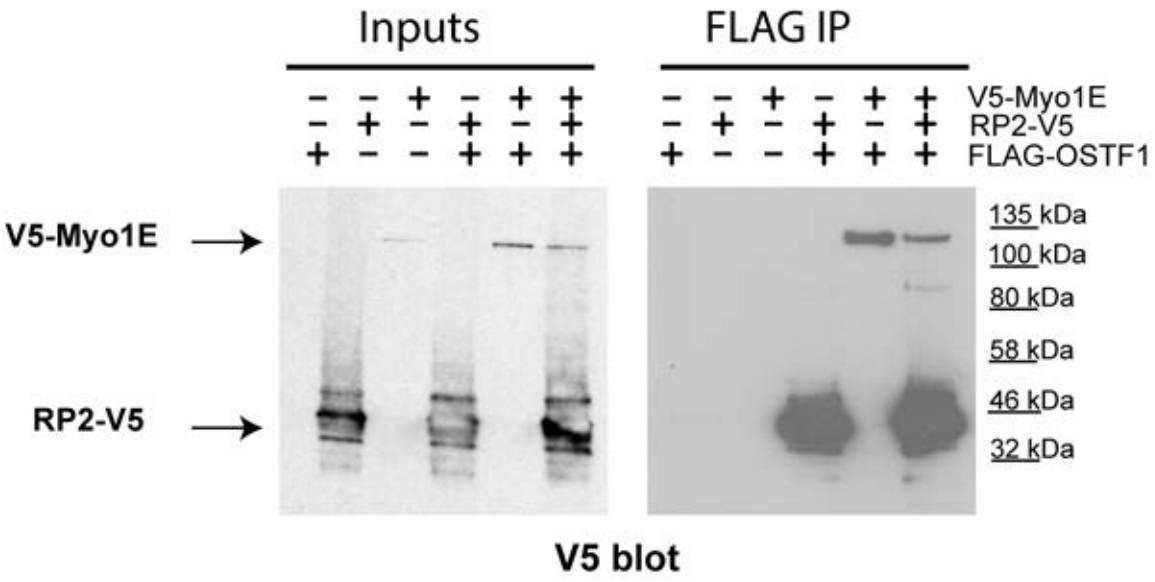

Supplementary figure 6. Full uncropped films corresponding to anti-V5 western blotting shown in figure 7c. HEK293T cells were transiently transfected with plasmids containing different combinations of V5-Myo1E, RP2-V5 and FLAG-OSTF1 constructs. The lysates were subjected to anti-FLAG IP to assess how much V5-Myo1E associated with FLAG-OSTF1 in the presence or absence of RP2-V5 overexpression, and immunoblotting using an antibody to V5 tag. The bands corresponding to V5-Myo1E and RP2-V5 are easily separated due to their completely different molecular weights.

Supplementary table 1. Equilibrium dissociation constants (Kd) of protein complexes (shown in brackets) in the presence or absence of other proteins, determined via fluorescence polarization (FP) or isothermal titration calorimetry (ITC).

Complex	Kd (µM)	Standard error	Method of determination
[1 µM ARL3-mantGppNHp – RP2]	0.092	0.077	FP
[1 µM ARL3-mantGDP-RP2]	6.137	1.667	FP
[1 µM ARL3-mantGppNHp – RP2] + OSTF1 (10 µM)	0.040	0.054	FP
[1 µM ARL3-mantGDP-RP2] + OSTF1 (10 µM)	6.967	1.117	FP
[1 µM ARL3-mantGppNHp – RP2] +UNC119a (4 µM)	0.082	0.133	FP
[RP2-OSTF1]	0.163	0.082	ITC
[1 µM RP2-OSTF1] + 1 µM ARL3-mantGppNHp	0.672	0.164	FP
[1 µM RP2-OSTF1] + 1 µM ARL3-mantGppNHp +2 µM UNC119a	0.235	0.145	FP

Supplementary table 2. Stability analysis of suggested RP2 mutations to probe OSTF1 interaction. FoldX[46,47] is applied to calculate the free energy difference between wild-type and mutant. The result is the free energy of mutation (ΔΔG) expressed in Kcal/mol; the mean of 10 calculation runs is reported. The error margin of FoldX is ~0.5 Kcal/mol so changes in that range are considered insignificant. The prediction decision is based upon [47,56,57] where: no effect on structural stability: ΔΔG <1.6 Kcal/mol, severely reduced structural stability: ΔΔG >1.6 Kcal/mol. Negative values indicate enhanced stabilities.

Mutation	Stability energy calculation on human unbound RP2 crystal structure (PDB ID: 2BX6) [Mean ΔΔG (kcal/mol)]	Stability energy calculation on human RP2-ARL3 crystal structure (PDB ID: 3BH7) [Mean ΔΔG (kcal/mol)]
K160A	0.31	0.24
K160E	0.30	0.14
E205A	-0.10	-0.05
E206A	0.27	-0.09
K208A	-0.34	-0.08
S213A	0.35	0.72
E215A	0.15	0.50
R218S	0.95	0.37
Y245A	0.48	0.72
K252A	0.66	0.73
D255A	-0.40	-0.58
E256A	0.04	-0.01